Available online at www.sciencedirect.com
SCIENCE DIRECT®
Journal of Sound and Vibration 280 (2005) 495–530
JOURNAL OF SOUND AND VIBRATION
www.elsevier.com/locate/jsvi

Frequency trimming of a vibrating ring-based multi-axis rate sensor

A.K. Rourke, S. McWilliam*, C.H.J. Fox

School of Mechanical, Materials, Manufacturing Engineering and Management, University of Nottingham, University Park, Nottingham NG7 2RD, UK

Received 6 October 2003; accepted 8 December 2003

Abstract

A recently proposed concept for a ring-based multi-axis rate sensor requires that two in-plane modes of vibration and two out-of-plane modes of vibration of a ring each have identical natural frequencies. This work proposes a practical mass trimming approach for eliminating the frequency splits between these four natural frequencies for an initially imperfect ring. Given that the modes of an imperfect ring are unlikely to consist of pure in-plane and pure out-of-plane modes, the proposed trimming approach takes account of the cross-coupling that exists between the in-plane and out-of-plane modes. The proposed approach consists of three stages: (i) eliminate the frequency split between a pair of predominantly in-plane modes and a pair of predominantly out-of-plane modes; (ii) eliminate the cross-coupling between the in-plane and out-of-plane modes; (iii) match the in-plane and out-of-plane natural frequencies. Numerical examples demonstrating and validating the approach are provided.

1. Introduction

The important drivers into the research and development of rate sensors are improvements in the accuracy, efficiency and useful measurement capability. A recently proposed concept for achieving such improvements is the multi-axis rate sensors; that is, a rate sensor that can detect the rotational speed of an object about more than one orthogonal axis simultaneously. Such sensors have the potential to reduce the need for increased numbers of single axis sensors and provide useful redundancy if a sensor fails.

The design of ring-based rate sensors is based around the fact that perfectly axi-symmetric rings have natural frequencies that occur in degenerate pairs and modes of vibration that are spatially

*Corresponding author. Fax: 0115-951-3800.
E-mail address: stewart.mcwilliam@nottingham.ac.uk (S. McWilliam).

0022-460X/$ - see front matter
doi:10.1016/j.jsv.2003.12.032

orthogonal and have indeterminate positions. Based on the planar form of rings, it is usual to refer to the modes of the ring as being either in-plane, consisting of radial and tangential displacements, or out-of-plane, consisting of axial (out-of-plane) and twisting displacements. To understand the principle of operation of a multi-axis sensor [1,2], consider the modes of vibration of a perfect ring shown in Fig. 1. The two pairs of modes on the left are in-plane modes and the two pairs of modes on the right are out-of-plane modes, both shown with 2 and 3 nodal diameters. If one of the in-plane modes is excited (the so-called carrier mode), angular rate about the polar axis will couple the in-plane (carrier) mode with the companion in-plane (response) mode. Applied rate about a diametral axis within the plane of the ring will couple the in-plane (carrier) mode with one or both of the out-of-plane (response) modes. Similarly, if one of the out-of-plane (carrier) modes is excited, angular rate about a diametral axis will couple the out-of-plane (carrier) mode with one or both of the in-plane (response) modes. More generally, it can be shown that the in-plane and out-of-plane modes only couple when $n_O = n_I \pm 1$ [1,2], where n_I is the number of in-plane nodal diameters and n_O is the number of out-of-plane nodal diameters. The coupling mechanism between the carrier and response modes is the Coriolis force and the sensitivity of the sensor is highly dependent on the natural frequencies of the modes concerned. To achieve maximum sensitivity of rate measurements, it is necessary to have the natural frequencies of the carrier mode and all of the response modes matched to within 0.01%. It is trivial to choose dimensions of a perfect ring to achieve this. However, in reality, imperfections due to dimensional variations and material non-uniformities exist which produce small frequency splits and severely diminish the performance.

The effect of imperfections is to introduce frequency splits both within a pair of "in-plane" and a pair of "out-of-plane" modes, and between the in-plane and out-of-plane modes. In addition, the imperfections fix the orientations of the modes within the ring. In previous work [1,2], the modes were assumed to be either in-plane or out-of-plane, even in the presence of imperfection. Strictly speaking this is not true, since any imperfection only slightly misaligned from the mid-surface of the plane of the ring will induce coupling between the in-plane and out-of-plane modes, modifying the mode shapes so that they each consist of a combination of in-plane and out-of-plane contributions. For a vibrating rate sensor, any imperfection-induced coupling can degrade the rate measurements, since the principle of operation is based on the coupling being due to the applied rate (through the Coriolis forces) only. Imperfect rings with high degrees of cross-coupling are a particular concern in the development of multi-axis rate sensors.

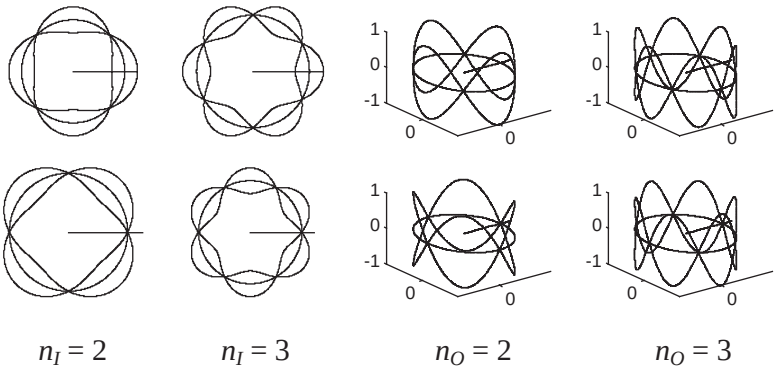

Fig. 1. The maximum displacements of the in-plane ($n_I = 2$ and 3) and out-of-plane ($n_O = 2$ and 3) generalized co-ordinates.

A number of researchers have reported the development of multi-axis rate sensors. Fujita et al. [3] proposed a two-axis sensor based on an oscillating disk that could measure rate about the axes within the plane of the disk. Work by Eley, Fox, McWilliam and Fell, in conjunction with BAE-Systems [1,2,4–6], has investigated the use of a ring-shaped rate sensor that can detect rate about two or three axes. The basic equations of motion have been derived and solved, and successful prototypes have been demonstrated. Gallacher et al. [7] have also reported work on ring sensors. These publications highlight the necessity for good frequency matching between modes, requiring trimming procedures to reduce (ideally eliminate) the effects of imperfection, but have not considered, in detail, the influence of imperfections, or how to compensate for them. The purpose of this paper is to investigate the effect of mass imperfections on the natural frequencies and orientations of the modes of a perfect ring and to develop a trimming process that can eliminate the aforementioned frequency splits from an imperfect ring by the addition, or removal, of mass.

The effect of imperfections on the in-plane modes of rings and cylinders has been studied by a number of authors [8–20]. Some papers [9,10,13,19,20] model imperfection in terms of masses and springs attached to the ring, while others [11,15–17] consider more general shape variations. As any manufacturing process has inherent errors that will introduce imperfections, it is necessary to consider methods for eliminating the effect of those imperfections. Useful papers by Fox [13,14] propose and demonstrate practical trimming procedures that can compensate for the effects of small imperfections and reduce the frequency split to an acceptable level for a single pair of modes. Rourke et al. [19,20] have extended this method to eliminate the frequency splits for multiple pairs of in-plane modes.

A similar approach will be taken here to investigate the effect of imperfections and to develop a trimming process to eliminate the effects of imperfections from four modes (one in-plane pair and one out-of-plane pair) with similar natural frequencies simultaneously. Section 2 will consider the effect of imperfection masses on the mode shapes and natural frequencies of a perfect ring, and also the cross-coupling between the in-plane and out-of-plane modes. In Section 3 a trimming procedure will be developed. This will consist of three stages: (i) the magnitude, radial and angular positions of the trimming masses will be determined to eliminate the frequency splits of the predominantly in-plane and out-of-plane modes; (ii) the axial positions of the same masses will be determined to eliminate the in-plane/out-of-plane coupling; (iii) the natural frequencies of the purely in-plane and out-of-plane trimmed modes will be matched by the addition of a second set of trimming masses. Section 4 will present some numerical examples to demonstrate and validate the derived trimming process.

2. Effect of imperfection masses on the modes of a perfect ring

Before outlining the effect of imperfection masses on a perfect ring, it is important to note that the perfect rings under consideration are thin. This ensures that the effects of rotary inertia and shear deformation are negligible and so these terms will not be considered in this analysis.

2.1. The in-plane and out-of-plane displacement of a ring

Previous work by the authors has considered the in-plane (tangential and radial) displacements (u, w) of a thin ring [19,20]. In this paper, the out-of-plane motion will also be considered. Using Kirkhope [21] the out-of-plane modes of a perfect ring consist of an axial displacement v and an

angular displacement θ, due to twisting about the centroidal axis of the ring section. These displacements are shown in Fig. 2.

In the present work, the displacement of the centre-line of the ring will be defined using four generalized co-ordinates, Q_i, where $i = I1$ and $I2$ correspond to the two orthogonal in-plane modes of a perfect ring that have n_I nodal diameters and $i = O1$ and $O2$ correspond to the two orthogonal out-of-plane modes that have n_O nodal diameters. As has been shown previously [22], the radial w and tangential u displacements associated with in-plane generalized co-ordinates Q_{I1}, Q_{I2} with n_I nodal diameters take the form

$$\begin{Bmatrix} w_{I1} \\ u_{I1} \end{Bmatrix} = Q_{I1}(t) \begin{Bmatrix} n_I \sin n_I(\phi - \varphi_{nI}) \\ \cos n_I(\phi - \varphi_{nI}) \end{Bmatrix}, \tag{1}$$

$$\begin{Bmatrix} w_{I2} \\ u_{I2} \end{Bmatrix} = Q_{I2}(t) \begin{Bmatrix} n_I \cos n_I(\phi - \varphi_{nI}) \\ -\sin n_I(\phi - \varphi_{nI}) \end{Bmatrix}, \tag{2}$$

and the axial displacement v and twisting θ about the centroidal axis associated with a pair of out-of-plane generalized co-ordinates Q_{O1}, Q_{O2} with n_O nodal diameters take the form

$$\begin{Bmatrix} v_{O1} \\ \theta_{O1} \end{Bmatrix} = Q_{O1}(t) \begin{Bmatrix} 1 \\ -n_O^2 \xi \end{Bmatrix} \cos n_O(\phi - \varphi_{nO}), \tag{3}$$

$$\begin{Bmatrix} v_{O2} \\ \theta_{O2} \end{Bmatrix} = Q_{O2}(t) \begin{Bmatrix} -1 \\ n_O^2 \xi \end{Bmatrix} \sin n_O(\phi - \varphi_{nO}), \tag{4}$$

where $\xi = ((1 + \mu)/(1 + n_O^2 \mu))/R$ and $\mu = GC_T/(EI_y)$. E, G and I_y are the Young's modulus, shear modulus and second moment of area of a section of the ring, $C_T = ch^3L^3/(h^2 + L^2)$ and c is a function of the ratio of h to L (radial thickness to axial length) that has values between 0.28 and 0.33 (see Table 8–18 of [22]). R is the mean radius of the ring (see Fig. 2).

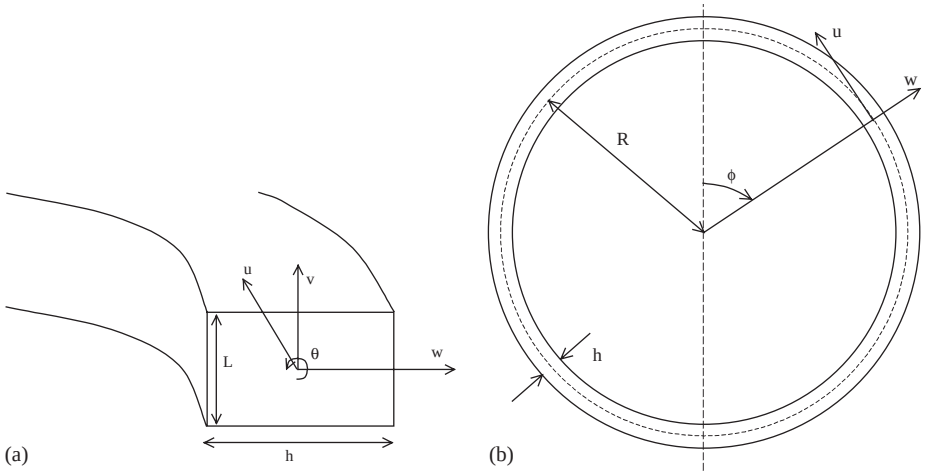

Fig. 2. (a) and (b) Dimensions and general co-ordinates of a ring.

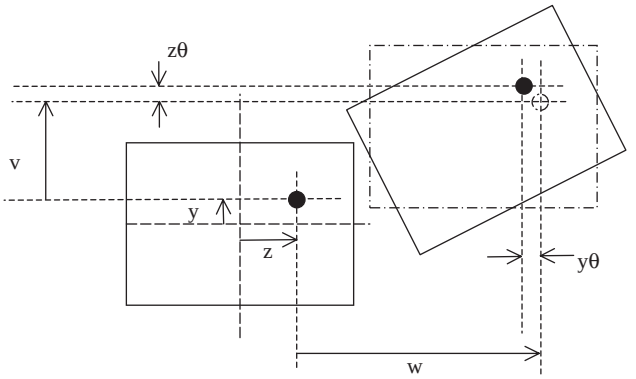

Fig. 3. Displacement of a general point of the ring.

The spatial angles φ_{nI} and φ_{nO} have been included to account for any possible misalignment between the in-plane and out-of-plane generalized co-ordinates and an arbitrary reference. It can be argued that, as the generalized co-ordinates can be chosen arbitrarily, these spatial angles are unnecessary. However, the generalized co-ordinates will be chosen so that each of the predominantly in-plane modes is aligned with one of the in-plane generalized co-ordinates and similarly each of the predominantly out-of-plane modes is aligned with one of the out-of-plane generalized co-ordinates. The reason for this choice is to simplify the analysis of the effect of imperfections and the trimming process. The introduction of spatial angles has been used in previous trimming processes [13,19,20].

Figs. 1(a) and (b) show the maximum displacements of the in-plane and out-of-plane generalized co-ordinates for n_I and n_O equal to 2 and 3, and include the undeformed ring and the $\phi = 0$ axis as reference points. The generalized co-ordinates have been chosen such that if Q_{I1} is orientated at angular position ϕ, the orthogonal co-ordinate Q_{I2} is orientated at $\phi + \pi/2n_I$ and similarly for Q_{O1} and Q_{O2}. In Figs. 1(a) and (b), Q_{I1} and Q_{O1} are aligned with each other at the arbitrary origin (in the sense that the corresponding radial and axial displacements have a cosine variation) but in general this will not be the case.

Taking into account the fact that the twisting θ produces displacement in the radial and axial direction for points not on the centre-line of the ring cross-section (see Fig. 3), it can be shown that the displacement of a general point in the cross-section of the ring can be expressed as

$$\begin{Bmatrix} u \\ v \\ w \end{Bmatrix} = Q_{I1} \begin{Bmatrix} \sin n_I(\phi - \varphi_{nI}) \\ 0 \\ n_I \cos n_I(\phi - \varphi_{nI}) \end{Bmatrix} + Q_{I2} \begin{Bmatrix} \cos n_I(\phi - \varphi_{nI}) \\ 0 \\ -n_I \sin n_I(\phi - \varphi_{nI}) \end{Bmatrix} + Q_{O1} \cos n_O(\phi - \varphi_{nO}) \begin{Bmatrix} 0 \\ 1 + z n_O^2 \xi \\ -y n_O^2 \xi \end{Bmatrix} + Q_{O2} \sin n_O(\phi - \varphi_{nO}) \begin{Bmatrix} 0 \\ 1 + z n_O^2 \xi \\ -y n_O^2 \xi \end{Bmatrix}, \tag{5}$$

where y and z are the axial and radial positions of the point under consideration.

2.2. General equations of motion of a perfect ring with attached point masses

The equations of motion for a perfect ring with attached point masses are derived using Lagrange's equations, and for this purpose it is necessary to consider the kinetic and strain energies of the structure.

It can be shown that the kinetic energy T of a perfect ring can be expressed as [23]

$$\begin{aligned} T &= \tfrac{1}{2}\rho hLR\pi\left((1+n_I^2)(\dot{Q}_{I1}^2+\dot{Q}_{I2}^2)+\left(1+\frac{(h^2+L^2)}{12}n_O^4\xi^2\right)(\dot{Q}_{O1}^2+\dot{Q}_{O2}^2)\right) \\ &= M_{I1}\dot{Q}_{I1}^2+M_{I2}\dot{Q}_{I2}^2+M_{O1}\dot{Q}_{O1}^2+M_{O2}\dot{Q}_{O2}^2, \end{aligned} \tag{6}$$

and the kinetic energy of the attached imperfection masses T_m can be expressed as

$$T_m = \tfrac{1}{2}\begin{pmatrix} m_{I1}\dot{Q}_{I1}^2+m_{I2}\dot{Q}_{I2}^2+m_{O1}\dot{Q}_{O1}^2+m_{O2}\dot{Q}_{O2}^2+\ 2m_{I1O1}\dot{Q}_{I1}\dot{Q}_{O1} \\ +2m_{I1O2}\dot{Q}_{I1}\dot{Q}_{O2}+2m_{I2O1}\dot{Q}_{I2}\dot{Q}_{O1}+2m_{I2O2}\dot{Q}_{I2}\dot{Q}_{O2} \end{pmatrix}, \tag{7}$$

where

$$m_{I1} = \sum_i m_i(\sin^2 n_I(\phi_i-\varphi_{n_I})+n_I^2\cos^2 n_I(\phi_i-\varphi_{n_I})), \tag{8}$$

$$m_{O1} = \sum_i m_i(1+2h_in_O^2\xi+(h_i^2+L_i^2)n_O^4\xi^2)\cos^2 n_O(\phi_i-\varphi_{n_O}), \tag{9}$$

$$m_{I2} = \sum_i m_i(\cos^2 n_I(\phi_i-\varphi_{n_I})+n_I^2\sin^2 n_I(\phi_i-\varphi_{n_I})), \tag{10}$$

$$m_{O2} = \sum_i m_i(1+2h_in_O^2\xi+(h_i^2+L_i^2)n_O^4\xi^2)\sin^2 n_O(\phi_i-\varphi_{n_O}), \tag{11}$$

$$m_{I1O1} = -n_In_O^2\xi\sum_i m_iL_i\cos n_I(\phi_i-\varphi_{n_I})\cos n_O(\phi_i-\varphi_{n_O}), \tag{12}$$

$$m_{I1O2} = -n_In_O^2\xi\sum_i m_iL_i\cos n_I(\phi_i-\varphi_{n_I})\sin n_O(\phi_i-\varphi_{n_O}), \tag{13}$$

$$m_{I2O1} = n_In_O^2\xi\sum_i m_iL_i\sin n_I(\phi_i-\varphi_{n_I})\cos n_O(\phi_i-\varphi_{n_O}), \tag{14}$$

$$m_{I2O1} = n_In_O^2\xi\sum_i m_iL_i\sin n_I(\phi_i-\varphi_{n_I})\sin n_O(\phi_i-\varphi_{n_O}). \tag{15}$$

In these equations, ρ is the density of the ring, h_i and L_i are the radial and axial locations of the ith attached imperfection mass from the centre of rotation, see z and y, respectively in Fig. 3, and ϕ_i is the angular location of the ith attached imperfection mass.

To determine expressions for the strain energy of the ring, it is assumed that the strain energies due to the in-plane and out-of-plane displacements can be calculated independently. It can be shown that the strain energy due to in-plane deformation can be expressed as [13]

$$S_{0n_I} = \frac{EhL\beta\pi}{2R(1-\nu^2)}n_I^2(1-n_I^2)^2(Q_{I1}^2+Q_{I2}^2) = \frac{K_{I1}}{2}Q_{I1}^2+\frac{K_{I2}}{2}Q_{I2}^2, \tag{16}$$

where $\beta = h^2/12R^2$ and v is the Poisson ratio. Using Ref. [21] it can be shown that the strain energy due to out-of-plane deformation can be expressed by

$$S_{0n_O} = \frac{EI_y}{2R}\int_0^{2\pi}\left(\frac{1}{R}\frac{\partial^2 v}{\partial\phi^2} - \theta\right)^2 \mathrm{d}\phi + \frac{C_T G}{2R}\int_0^{2\pi}\left(\frac{\partial\theta}{\partial\phi} + \frac{1}{R}\frac{\partial v}{\partial\phi}\right)^2 \mathrm{d}\phi, \tag{17}$$

where the effects of twisting have been included. Substituting Eqs. (3) and (4) into Eq. (17) gives

$$S_{0n_O} = \frac{EI_y\pi}{2R^3}\frac{n_O^2(n_O^2-1)^2\mu}{(1+n_O^2\mu)}(Q_{O1}^2 + Q_{O2}^2) = \frac{K_{O1}}{2}Q_{O1}^2 + \frac{K_{O2}}{2}Q_{O2}^2. \tag{18}$$

As in previous mass trimming processes [13,19,20], it will be assumed that the mass imperfections do not affect the stiffness of the ring.

Combining Eqs. (6) and (7) to obtain the total kinetic energy and Eqs. (16) and (18) to obtain the total strain energy, and substituting the resulting expressions into Lagrange's equation together with a standard viscous dissipation function yields the following equations of motion:

$$(\mathbf{M}+\mathbf{m})\ddot{\mathbf{Q}} + \mathbf{C}\dot{\mathbf{Q}} + \mathbf{K}\mathbf{Q} = \mathbf{F}, \tag{19}$$

where

$$\mathbf{M} = \mathrm{diag}[M_{I1}, M_{I2}, M_{O1}, M_{O2}],$$
$$\mathbf{K} = \mathrm{diag}[K_{I1}, K_{I2}, K_{O1}, K_{O2}],$$
$$\mathbf{C} = \mathrm{diag}[C_{I1}, C_{I2}, C_{O1}, C_{O2}],$$
$$\mathbf{m} = \begin{bmatrix} m_{I1} & 0 & m_{I1O1} & m_{I1O2} \\ 0 & m_{I2} & m_{I2O1} & m_{I2O2} \\ m_{I1O1} & m_{I2O1} & m_{O1} & 0 \\ m_{I1O2} & m_{I2O2} & 0 & m_{O2} \end{bmatrix}, \tag{20–23}$$

$$\mathbf{F} = (F_{I1} \quad F_{I2} \quad F_{O1} \quad F_{O2})^{\mathrm{T}}, \quad \mathbf{Q} = (Q_{I1} \quad Q_{I2} \quad Q_{O1} \quad Q_{O2})^{\mathrm{T}}, \tag{24,25}$$

where $\mathrm{diag}[a_1, a_2, \ldots, a_n]$ represents an $n \times n$ diagonal matrix whose ijth entry is a_k when $i = j = k$ and 0 when $i \neq j$. Here F_k and C_k are the external forces and damping terms associated with generalized co-ordinates Q_k.

It can be seen from the off-diagonal terms in the mass matrix $\mathbf{m}$ that, in general, the in-plane and out-of-plane generalized co-ordinates are coupled. Using Eqs. (12)–(15) it can be seen that the coupling due to an *individual* imperfection mass is dependent on the size and location of the mass, and on the displacement of the ring at the point of attachment. Furthermore, the off-diagonal mass terms will affect the natural frequencies and modes of vibration of the ring. The influence of the coupling on the natural frequencies and mode shapes will be discussed with reference to an example in what follows.

2.3. Natural frequencies and modes of vibration for an example imperfect ring

To illustrate the effect of imperfection masses on the natural frequencies and mode shapes of the ring, a numerical example will now be considered consisting of a pair of imperfection masses attached to a perfect ring. The dimensions and physical properties of the ring are chosen to be in agreement with the prototype multi-axis ring that was designed by Eley [2] to produce natural frequencies of approximately 4 kHz for the $n_I = 2$ in-plane modes and the $n_O = 3$ out-of-plane modes. The density of the ring $\rho = 8250\ \mathrm{kg/m^3}$, the mean radius $R = 0.0415$ m, the radial thickness $h = 0.003$ m, the axial length $L = 0.00105$ m, and the value of $\mu = 0.3$. From these

properties the mass matrix **M** of the perfect ring (see Eq. (20)) can be calculated. In the results that follow, the stiffness is chosen to produce an out-of-plane natural frequency ω_{0O} of 4004 Hz and an in-plane natural frequency ω_{0I} between 4000 and 4010 Hz for the perfect ring. Thus the stiffness matrix **K** of the perfect ring is generated by using Eq. (21) and by noting that the natural frequencies of the perfect ring are given by $\omega^2 = S/T$.

The effect on the perfect ring of a pair of imperfection masses of 0.1% and 0.15% of the mass of the perfect ring, attached at angular positions of 0° and 30°, respectively, and at radial and axial positions of $-h/2$ and $L/2$ from the centre-line of the ring will be considered. Figs. 4(a)–(d) shows the eigenvectors, whilst Fig. 4(e) shows the natural frequencies for these specified imperfections.

Figs. 4(a)–(d) represent the relative contributions of the two in-plane and two out-of-plane generalized co-ordinates for each mode. It can be seen that there are no modes that are purely in-plane or purely out-of-plane as the natural frequencies of the perfect ring are varied. Instead, all four mode shapes are a combination of in-plane and out-of-plane contributions. This is particularly apparent in regions where the natural frequencies of the modes are close together (see Fig. 4(e)).

Fig. 4(e) shows the natural frequencies of the ring. The solid curves represent the exact natural frequencies, whilst the dashed curves indicate the natural frequencies of the ring if there was no coupling between the in-plane and out-of-plane displacement, i.e., if the off-diagonal terms m_{I1O1}, m_{I1O2}, m_{I2O1} and m_{I2O2} are neglected in Eq. (23). It can be seen that there are some combinations of in-plane and out-of-plane frequencies of a perfect ring for which a single "in-plane" natural frequency and a single "out-of-plane" natural frequency are the same when the imperfection masses are added. For these situations, the natural frequencies cannot be determined accurately by neglecting the off-diagonal mass terms. Similarly, the modes at those points cannot be considered as being purely "in-plane" or purely "out-of-plane".

For regions where the natural frequencies are not close together (for example, the regions close to 4000 and 4010 Hz) it can be seen that the mode shapes correspond to either in-plane or out-of-plane modes, meaning that the equations of motion are effectively uncoupled. In addition, in these regions, the effect of the in-plane/out-of-plane coupling on the natural frequencies of the modes becomes negligible, and the modal behaviour is greatly simplified. It is in these regions that previous analysis of the effect of imperfections on the modes of a ring was performed.

2.4. Some comments on the development of a multi-axis trimming procedure

Previous work on frequency trimming has considered trimming in-plane and out-of-plane modes that are uncoupled. Given that these mode types are effectively uncoupled when their natural frequencies are sufficiently separated, a sensible strategy in the development of a practical trimming procedure is to: (i) consider a ring in which the in-plane and out-of-plane natural frequencies are sufficiently separated that the in-plane/out-of-plane coupling can be ignored, and trim the in-plane and out-of-plane modes separately; (ii) eliminate the in-plane/out-of-plane coupling; (iii) trim the uncoupled ring so that the in-plane natural frequencies are equal to the out-of-plane natural frequencies. To achieve steps (i) and (ii) it is necessary to consider the effects of imperfection masses on: (i) the natural frequencies of the ring when the coupling is neglected; and (ii) the coupling between the in-plane and out-of-plane modes. These are considered in the following sections.

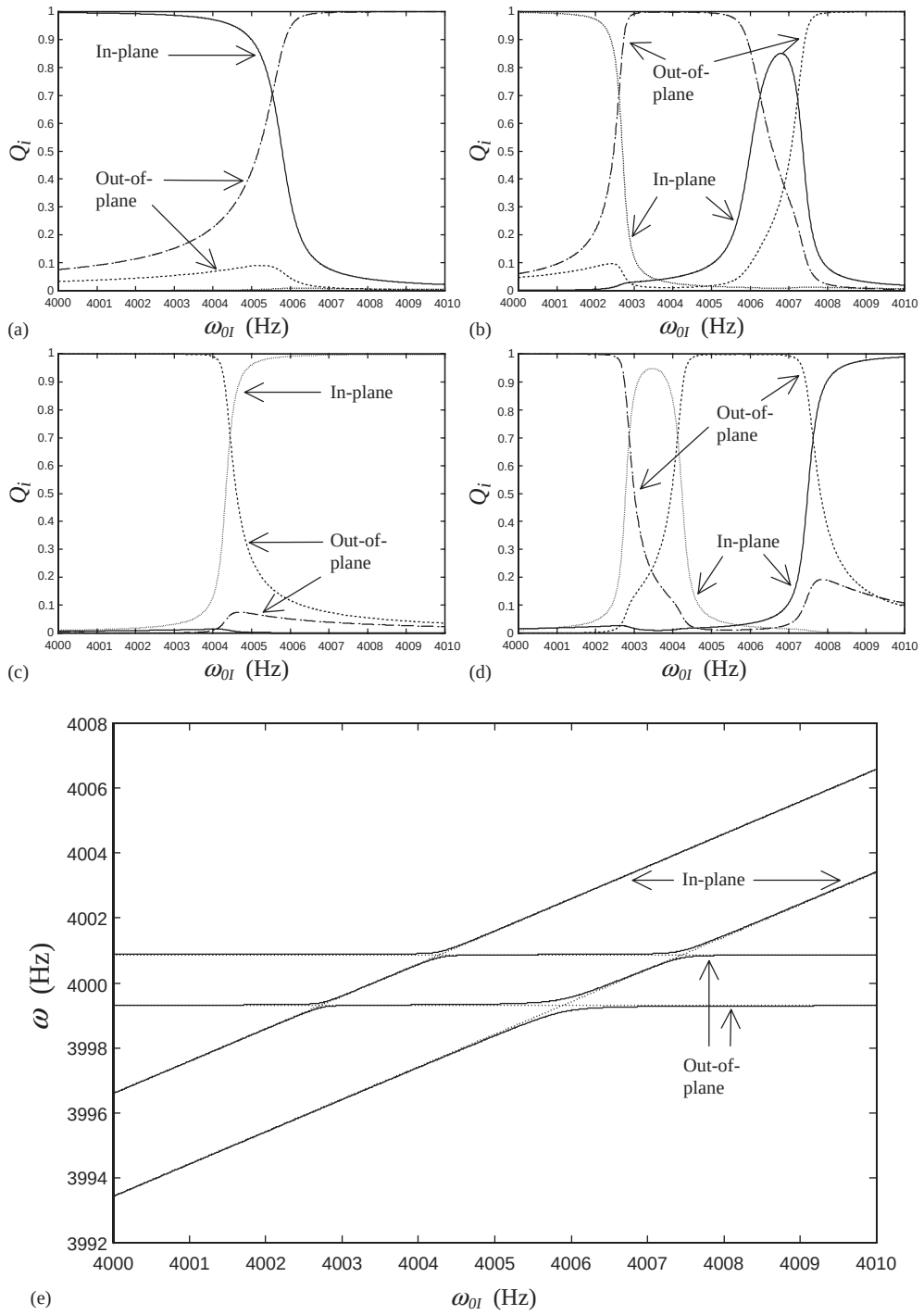

Fig. 4. (a)–(d) In-plane and out-of-plane displacements of the four modes of an imperfect ring that has been formed by the addition of a pair of imperfection masses. (e) Natural frequencies of the four modes of an imperfect ring that has been formed by the addition of a pair of imperfection masses.

2.5. Natural frequencies for an imperfect ring, neglecting in-plane/out-of-plane coupling

Neglecting the in-plane/out-of-plane coupling, the natural frequencies for a perfect ring with attached point masses can be determined using Eq. (19), but with the off-diagonal terms m_{I1O1}, m_{I1O2}, m_{I2O1} and m_{I2O2} set to zero in Eq. (23). Noting that Eq. (19) is uncoupled, it is a reasonably simple task to calculate the natural frequencies analytically, and it can be shown that the in-plane and out-of-plane natural frequencies are given by

$$\omega^2_{\substack{I1\\I2}} = \omega^2_{0I}\left(\frac{1+n_I^2}{(1+n_I^2)+\sum_i m_i[(1+n_I^2)\pm(n_I^2-1)\cos 2n_I(\phi_i-\varphi_{n_I})]/M_0}\right), \tag{26}$$

$$\omega^2_{\substack{O1\\O2}} = \omega^2_{0O}\left(\frac{(1+\frac{h^2+L^2}{12}n_O^4\xi^2)}{(1+\frac{h^2+L^2}{12}n_O^4\xi^2)+\sum_i m_i(1+2h_in_O^2\xi+(h_i^2+L_i^2)n_O^4\xi^2)(1\pm\cos 2n_O(\phi_i-\varphi_{n_O}))/M_0}\right), \tag{27}$$

where ω_{0I} and ω_{0O} are the in-plane and out-of-plane natural frequencies for the perfect ring, such that

$$\omega^2_{0I} = \frac{K_{I1}}{M_{I1}} = \frac{K_{I2}}{M_{I2}} = \frac{E\beta n_I^2(1-n_I^2)^2}{R^2\rho(1-\nu^2)(1+n_I^2)}, \tag{28}$$

$$\omega^2_{0O} = \frac{K_{O1}}{M_{O1}} = \frac{K_{O2}}{M_{O2}} = \frac{2EI_y\pi}{M_0R^3}\frac{n_O^2(n_O^2-1)^2\mu}{(1+n_O^2\mu)(1+\frac{h^2+L^2}{12}n_O^4\xi^2)}. \tag{29}$$

In addition, it can be shown [13] that the orientations of the in-plane and out-of-plane modes (φ_{nI} and φ_{nO} in Eqs. (1)–(4)) with respect to some general reference point can be determined, and are given by

$$\tan 2n_I\varphi_{n_I} = \frac{\sum_i m_i \sin 2n_I\phi_i}{\sum_i m_i\cos 2n_I\phi_i}, \tag{30}$$

$$\tan 2n_O\varphi_{n_O} = \frac{\sum_i m_i(1+2h_in_O^2\xi+(h_i^2+L_i^2)n_O^4\xi^2)\sin 2n_O\phi_i}{\sum_i m_i(1+2h_in_O^2\xi+(h_i^2+L_i^2)n_O^4\xi^2)\cos 2n_O\phi_i}. \tag{31}$$

Eqs. (26)–(31) are expressions for the natural frequencies and mode orientations for a perfect ring with attached point masses, assuming that there is no coupling between the in-plane/out-of-plane modes. These equations will be used to formulate part of the proposed trimming procedure later.

2.6. In-plane/out-of-plane coupling for an imperfect ring

To be able to develop a practical trimming process it is necessary to eliminate the effects of cross-coupling between the in-plane and out-of-plane modes. To be able to achieve this it is necessary to be able to quantify the amount of cross-coupling that exists, and this is considered here.

In practice, the influence of cross-coupling is most apparent in a vibrating gyroscope when harmonic excitation applied to an in-plane mode (say) results in a harmonic out-of-plane response, when no rate is applied. For this reason, it is convenient to consider the response of the generalized co-ordinates when a harmonic excitation is applied to the system.

Applying a harmonic excitation at frequency ω to Eq. (19), the steady state response of the generalized co-ordinates can be expressed as

$$Q_{I1} = q_{I1}\sin(\omega t - \Psi_{I1}), \quad Q_{I2} = q_{I2}\sin(\omega t - \Psi_{I2}),$$
$$Q_{O1} = q_{O1}\sin(\omega t - \Psi_{O1}), \quad Q_{O2} = q_{O2}\sin(\omega t - \Psi_{O2}), \tag{32–35}$$

where the Ψ_k terms take account of the phase differences between the generalized co-ordinates and the excitation force. Substituting Eqs. (32)–(35) into the equation of motion (19) produces equations of the following form

$$\{(\omega_k^2 - \omega^2)\sin(\omega t - \Psi_k) + 2\omega\omega_k\gamma_k\cos(\omega t - \Psi_k)\}q_k - \frac{\omega^2}{M_k + m_k}(m_{kd1}q_{d1}\sin(\omega t - \Psi_{d1}) + m_{kd2}q_{d2}\sin(\omega t - \Psi_{d2})) = \frac{F_k}{M_k + m_k}\sin\omega t, \tag{36}$$

where if $k = I1$ or $I2$, $d = O$ and if $k = O1$ or $O2$, $d = I$, $m_{kd1} = m_{d1k}$ and $m_{kd2} = m_{d2k}$. In addition, ω_k is given by Eqs. (26) and (27) and $2\omega_k\gamma_k = C_k/(M_k + m_k)$.

Solving Eq. (36) it can be shown that the magnitude and phase of the generalized co-ordinates are given by

$$q_k = \frac{\left\{\begin{array}{l}\left((\omega_k^2 - \omega^2)F_k + \omega^2\left(\begin{array}{l}(\omega_k^2 - \omega^2)m_{kd1}q_{d1}\cos\Psi_{d1} - 2\omega\omega_k\gamma_k m_{kd1}q_{d1}\sin\Psi_{d1}\\ \quad + (\omega_k^2 - \omega^2)m_{kd2}q_{d2}\cos\Psi_{d2} - 2\omega\omega_k\gamma_k m_{kd2}q_{d2}\sin\Psi_{d2}\end{array}\right)\right)^2\\ \quad + \left(2\omega\omega_k\gamma_k F_k + \omega^2\left(\begin{array}{l}(\omega_k^2 - \omega^2)m_{kd1}q_{d1}\sin\Psi_{d1} + 2\omega\omega_k\gamma_k m_{kd1}q_{d1}\cos\Psi_{d1}\\ \quad + (\omega_k^2 - \omega^2)m_{kd2}q_{d2}\sin\Psi_{d2} + 2\omega\omega_k\gamma_k m_{kd2}q_{d2}\cos\Psi_{d2}\end{array}\right)\right)^2\end{array}\right\}^{1/2}}{(M_k + m_k)((\omega_k^2 - \omega^2)^2 + 4\omega^2\omega_k^2\gamma_k^2)}, \tag{37}$$

$$\tan\Psi_k = \frac{2\omega\omega_k\gamma_k F_k + \omega^2\left(\begin{array}{l}(\omega_k^2 - \omega^2)m_{kd1}q_{d1}\sin\Psi_{d1} + 2\omega\omega_k\gamma_k m_{kd1}q_{d1}\cos\Psi_{d1}\\ \quad + (\omega_k^2 - \omega^2)m_{kd2}q_{d2}\sin\Psi_{d2} + 2\omega\omega_k\gamma_k m_{kd2}q_{d2}\cos\Psi_{d2}\end{array}\right)}{(\omega_k^2 - \omega^2)F_k + \omega^2\left(\begin{array}{l}(\omega_k^2 - \omega^2)m_{kd1}q_{d1}\cos\Psi_{d1} - 2\omega\omega_k\gamma_k m_{kd1}q_{d1}\sin\Psi_{d1}\\ \quad + (\omega_k^2 - \omega^2)m_{kd2}q_{d2}\cos\Psi_{d2} - 2\omega\omega_k\gamma_k m_{kd2}q_{d2}\sin\Psi_{d2}\end{array}\right)}. \tag{38}$$

It is clear from Eqs. (37) and (38) that the generalized co-ordinates are coupled, and that it is difficult to obtain exact analytical expressions for the generalized co-ordinates that are independent of the other generalized co-ordinates—i.e., Eqs. (37) and (38) are non-linear algebraic equations in terms of the generalized co-ordinates and the associated phase angles. An iterative solution for the generalized co-ordinates and phase angles is feasible and is used here to develop an approximate analytical solution to these equations. This is achieved by using a two-step iterative solution procedure. The first step assumes that the coupling has no effect on the solution, and yields an approximate (first order) solution for the generalized co-ordinates and

phase angles. This solution is equivalent to neglecting the "$\omega^2(\ldots)$" terms appearing on the right hand sides of Eqs. (37) and (38). The second step involves using these first order solutions in the right hand side of Eqs. (37) and (38) to determine a new approximate solution. Performing this operation it can be shown that the generalized co-ordinates and the associated phase angles can be expressed as

$$q_k = \frac{(H_{3k}^2 + H_{4k}^2)^{1/2}}{(M_k + m_k)\{(\omega_k^2 - \omega^2)^2 + 4\omega^2\omega_k^2\gamma_k^2\}}, \quad \tan \Psi_k = \frac{H_{4k}}{H_{3k}}, \tag{39, 40}$$

where

$$H_{3k} = H_{1k} + \frac{m_{kd1}}{(M_{d1} + m_{d1})} \frac{\omega^2((\omega_k^2 - \omega^2)H_{1d1} - 2\omega\omega_k\gamma_k H_{2d1})}{(\omega_{d1}^2 - \omega^2)^2 + 4\omega^2\omega_{d1}^2\gamma_{d1}^2} + \frac{m_{kd2}}{(M_{d2} + m_{d2})} \frac{\omega^2((\omega_k^2 - \omega^2)H_{1d2} - 2\omega\omega_k\gamma_k H_{2d2})}{(\omega_{d2}^2 - \omega^2)^2 + 4\omega^2\omega_{d2}^2\gamma_{d2}^2}, \tag{41}$$

$$H_{4k} = H_{2k} + \frac{m_{kd1}}{(M_{d1} + m_{d1})} \frac{\omega^2(2\omega\omega_k\gamma_k H_{1d1} + (\omega_k^2 - \omega^2)H_{2d1})}{(\omega_{d1}^2 - \omega^2)^2 + 4\omega^2\omega_{d1}^2\gamma_{d1}^2} + \frac{m_{kd2}}{(M_{d2} + m_{d2})} \frac{\omega^2(2\omega\omega_k\gamma_k H_{1d2} + (\omega_k^2 - \omega^2)H_{2d2})}{(\omega_{d2}^2 - \omega^2)^2 + 4\omega^2\omega_{d2}^2\gamma_{d2}^2}, \tag{42}$$

$$H_{1k} = (\omega_k^2 - \omega^2)F_k, \quad H_{2k} = 2\omega\omega_k\gamma_k F_k. \tag{43, 44}$$

Eqs. (39) and (40) indicate how the generalized co-ordinates depend on their associated ω_k terms, the imperfections masses attached to the ring and the frequency of the applied driving forces ω. By considering only a single force, it is possible to evaluate the degree of in-plane/out-of-plane coupling that exists in each mode of the imperfect ring. To achieve this for a practical vibrating rate sensor it is necessary to consider the practical arrangement of drive forces and sensors that are used. This will be considered next.

2.7. In-plane/out-of-plane coupling of a practical sensor

In a typical sensor structure, sensors measuring the radial motion of the ring determine the displacements of the in-plane modes and sensors measuring the motion perpendicular to the plane of the ring determine the displacements of the out-of-plane modes. There will be a reference point within the ring that is fixed by the structure of the ring. The position of the in-plane and out-of-plane modes, and so the positions of the generalized co-ordinates, will be determined with reference to that point using these in-plane and out-of-plane sensors.

If the in-plane and out-of-plane sensors are positioned at angular locations ϕ_{pi} and ϕ_{po}, respectively (see Fig. 5), then the radial and axial displacements "seen" by the sensors can be expressed as

$$\begin{aligned} w &= w_{I1}Q_{I1} + w_{I2}Q_{I2} \\ &= n_I(q_{I1}\sin(\omega t - \Psi_{I1})\cos n_I(\phi_{pi} - \varphi_{n_I}) - q_{I2}\sin(\omega t - \Psi_{I2})\sin n_I(\phi_{pi} - \varphi_{n_I})) \\ &= W\sin(\omega t - \Psi_W), \end{aligned} \tag{45}$$

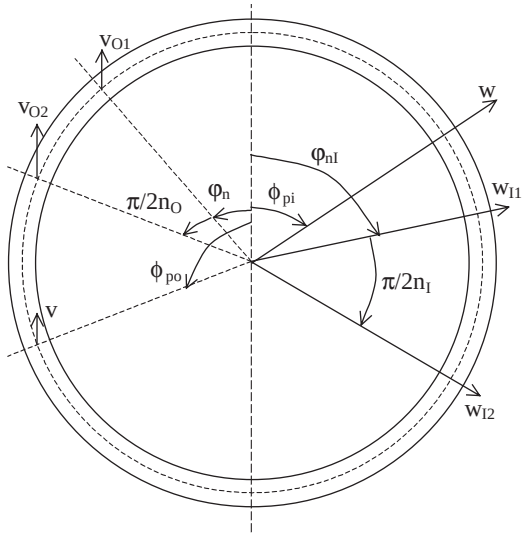

Fig. 5. Orientation of the in-plane and out-of-plane generalized co-ordinates within the ring with respect to an arbitrary origin and the orientation of the in-plane and out-of-plane sensors with respect to the same origin.

$$\begin{aligned} v &= v_{O1}Q_{O1} + v_{O2}Q_{O2} \\ &= q_{O1}\sin(\omega t - \Psi_{O1})\cos n_O(\phi_{po} - \varphi_{n_O}) - q_{O2}\sin(\omega t - \Psi_{O2})\sin n_O(\phi_{po} - \varphi_{n_O}) \\ &= V\sin(\omega t - \Psi_V), \end{aligned} \tag{46}$$

where

$$W = n_I\left(\begin{array}{l}(q_{I1}\cos\Psi_{I1}\cos n_I(\phi_{pi} - \varphi_{n_I}) - q_{I2}\cos\Psi_{I2}\sin n_I(\phi_{pi} - \varphi_{n_I}))^2 \\ \quad + (q_{I1}\sin\Psi_{I1}\cos n_I(\phi_{pi} - \varphi_{n_I}) - q_{I2}\sin\Psi_{I2}\sin n_I(\phi_{pi} - \varphi_{n_I}))^2\end{array}\right)^{1/2}, \tag{47}$$

$$\tan\Psi_W = \frac{q_{I1}\sin\Psi_{I1}\cos n_I(\phi_{pi} - \varphi_{n_I}) - q_{I2}\sin\Psi_{I2}\sin n_I(\phi_{pi} - \varphi_{n_I})}{q_{I1}\cos\Psi_{I1}\cos n_I(\phi_{pi} - \varphi_{n_I}) - q_{I2}\cos\Psi_{I2}\sin n_I(\phi_{pi} - \varphi_{n_I})}, \tag{48}$$

$$V = \left(\begin{array}{l}(q_{O1}\cos\Psi_{O1}\cos n_O(\phi_{po} - \varphi_{n_O}) - q_{O2}\cos\Psi_{O2}\sin n_O(\phi_{po} - \varphi_{n_O}))^2 \\ \quad + (q_{O1}\sin\Psi_{O1}\cos n_O(\phi_{po} - \varphi_{n_O}) - q_{O2}\sin\Psi_{O2}\sin n_O(\phi_{po} - \varphi_{n_O}))^2\end{array}\right)^{1/2}, \tag{49}$$

$$\tan\Psi_V = \frac{q_{O1}\sin\Psi_{O1}\cos n_O(\phi_{po} - \varphi_{n_O}) - q_{O2}\sin\Psi_{O2}\sin n_O(\phi_{po} - \varphi_{n_O})}{q_{O1}\cos\Psi_{O1}\cos n_O(\phi_{po} - \varphi_{n_O}) - q_{O2}\cos\Psi_{O2}\sin n_O(\phi_{po} - \varphi_{n_O})}. \tag{50}$$

In general, $\phi_{pi} \neq \varphi_{n_I}$ or $\varphi_{n_I} + \pi/2n_I$ and $\phi_{po} \neq \varphi_{n_O}$ or $\varphi_{n_{IO}} + \pi/2n_O$ and so the sensors will measure a combination of the displacements along both of the relevant generalized co-ordinates (in-plane generalized co-ordinates with the in-plane sensor and out-of-plane generalized co-ordinates with the out-of-plane sensor). As the modes and the generalized co-ordinates are orientated at the same

position this means that, in general, the sensors will measure a combination of the displacements of more than one mode. However, if the sensors are aligned with the position of one of the relevant generalized co-ordinates then only the displacement of the corresponding mode (such as the first in-plane mode) will be measured and none of the other mode (the second in-plane mode) will be detected.

Eqs. (45) and (46) enable the magnitude of the coupling between the in-plane and out-of-plane generalized co-ordinates to be assessed. This process can be simplified further by considering specific forces associated with specific generalized co-ordinates. For example, consider an applied force F_{I1} with the forces associated with the other three generalized co-ordinates set equal to zero. For this case, Eqs. (45) and (46) simplify to

$$W = \frac{n_I F_{I1} \cos n_I(\phi_{pi} - \varphi_{n_I})}{(M_{I1} + m_{I1})((\omega_{I1}^2 - \omega^2)^2 + 4\omega^2\omega_{I1}^2\gamma_{I1}^2)^{1/2}}, \tag{51}$$

$$V = \frac{F_{I1}\omega^2}{(M_{I1} + m_{I1})((\omega_{I1}^2 - \omega^2)^2 + 4\omega^2\omega_{I1}^2\gamma_{I1}^2)^{1/2}} \times \left(\begin{array}{c} (B_{I1O1}\cos\Psi_{O1} - B_{I1O2}\cos\Psi_{O2})^2 \\ +(B_{I1O1}\sin\Psi_{O1} - B_{I1O2}\sin\Psi_{O2})^2 \end{array} \right)^{1/2}, \tag{52}$$

where

$$\tan\Psi_{Oj} = 2\omega\left(\frac{\omega_{I1}\gamma_{I1}(\omega_{Oj}^2 - \omega^2) + \omega_{Oj}\gamma_{Oj}(\omega_{I1}^2 - \omega^2)}{(\omega_{I1}^2 - \omega^2)(\omega_{Oj}^2 - \omega^2) - 4\omega^2\omega_{I1}\omega_{Oj}\gamma_{I1}\gamma_{Oj}}\right), \tag{53}$$

$$B_{kO1} = \frac{m_{kO1}\cos n_O(\phi_{po} - \varphi_{n_O})}{(M_{O1} + m_{O1})((\omega_{O1}^2 - \omega^2)^2 + 4\omega^2\omega_{O1}^2\gamma_{O1}^2)^{1/2}}, \tag{54}$$

$$B_{kO2} = \frac{m_{kO2}\sin n_O(\phi_{po} - \varphi_{n_O})}{(M_{O2} + m_{O2})((\omega_{O2}^2 - \omega^2)^2 + 4\omega^2\omega_{O2}^2\gamma_{O2}^2)^{1/2}}. \tag{55}$$

There are a number of features of Eqs. (51) and (52) that will be relevant when considering the trimming of the frequency splits of an imperfect ring with the additional aim of eliminating in-plane/out-of-plane coupling. The main point to note is the dependence of Eq. (52) on the mass terms, m_{I1O1} and m_{I1O2}. These terms will have a significant effect on the in-plane/out-of-plane coupling. For example, if both of these terms could be reduced to zero there would be no coupling. Also, if the net contribution from the mass terms was zero in Eq. (52), then there would be no coupling. Expressions for the mass terms were given in Eqs. (12–15) and it can be seen that the terms are linearly dependent on the mass and the axial positions of the imperfection masses but are independent of their radial positions. Therefore, it is possible to modify the degree of in-plane/out-of-plane coupling for specific imperfection masses by varying the axial positions of the masses only. This will be significant in the trimming process.

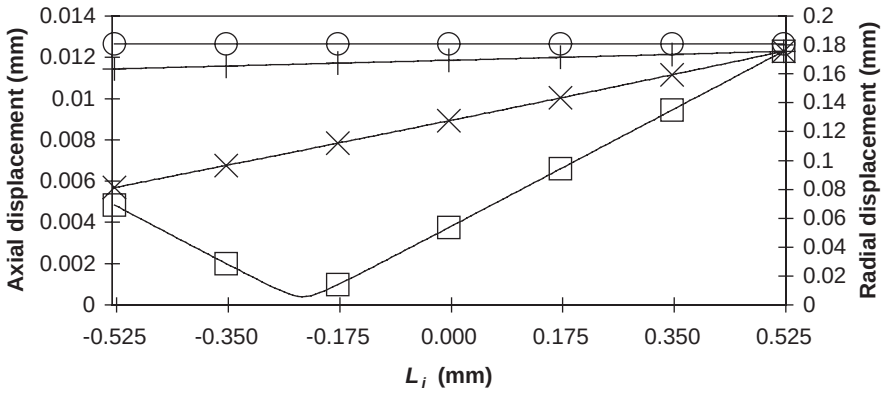

Fig. 6. Variation in the coupling between the in-plane and out-of-plane generalized co-ordinates due to variation in the axial position of the imperfection mass for the case of three mass imperfections (○, W; □, V for variations in L_1; +, V for variations in L_2; ×, V for variations in L_3).

The effect on the in-plane/out-of-plane coupling is illustrated in Fig. 6 by varying the axial positions of three imperfection masses (of 0.1%, 0.2% and 0.3% of the mass of the perfect ring at 0°, 35° and 70°, respectively and radial distances of $-h/2$). If the axial position of a specific mass is not being varied it is kept constant at $L/2$. To produce Fig. 6, the ring was excited at the natural frequency of the predominantly in-plane mode. It can be seen that varying the axial positions of the different masses will have different effects on the coupling. In particular, there is an arrangement of imperfection masses (m_1 at approximately $-2L/5$ and m_2 and m_3 at $L/2$) that produces no in-plane/out-of-plane coupling. Thus, it is possible that the imperfections may be arranged to produce no in-plane/out-of-plane coupling and so inversely it is implied that trimming masses can be applied to nullify the effect of the imperfections.

In summary, it has been shown that the angular positions of the in-plane and out-of-plane sensors will have a significant effect on the level of in-plane/out-of-plane coupling that is measured at different driving frequencies. It has also been shown that the axial distances of the imperfections from the centre-line of the cross-section of the ring have a significant effect on the coupling and that it is possible for there to be combinations of imperfections masses offset from the centre-line that do not introduce an overall in-plane/out-of-plane coupling.

3. Trimming process

In Section 2, the effect of imperfection masses on the in-plane and out-of-plane modes of a perfect ring was considered. It was shown that the imperfection masses introduce frequency splits and fix the orientations of the in-plane and out-of-plane modes. In addition, it was shown that imperfections not located within the central plane of the ring induce cross-coupling between the in-plane and out-of-plane modes, and that the modes can no longer be treated as being purely in-plane or purely out-of-plane. Indeed, it is possible that the modes are a complex combination of in-plane and out-of-plane contributions.

Mass trimming is the attachment or removal of mass to eliminate or at least reduce the frequency splits between the modes of interest. The analysis described in Section 2 can be used to achieve this by identifying the magnitudes and locations of equivalent imperfection masses that give the same frequency splits and mode orientations as those observed for an imperfect ring [13,19,20]. By removing these masses from the imperfect ring it is possible to eliminate the frequency splits.

In what follows, a three stage trimming procedure is proposed. Stage 1 considers the trimming of a pair of predominantly in-plane and a pair of predominantly out-of-plane modes. Stage 2 eliminates the in-plane/out-of-plane coupling. Stage 3 matches the in-plane and out-of-plane natural frequencies. Each of these stages is considered in turn as follows.

3.1. Stage 1. Eliminating the frequency splits between a pair of predominantly in-plane and a pair of predominantly out-of-plane modes of vibration

Eqs. (26) and (30) relate attached masses and their angular positions to the split natural frequencies and orientations of predominantly in-plane modes of an imperfect ring. Using previous work by the authors, these equations can be re-written as

$$\sum_i m_i \sin 2n_I(\phi_i - \varphi_{n_I}) = 0, \quad \sum_i m_i \cos 2n_I(\phi_i - \varphi_{n_I}) = M\lambda_{n_I}, \tag{56, 57}$$

where $\lambda_{n_I} = (\omega_{I1}^2 - \omega_{I2}^2)(1 + n_I^2)/((\omega_{I1}^2 + \omega_{I2}^2)(1 - n_I^2))$ and M is the mass of the imperfect ring.

A similar pair of equations can be produced for predominantly out-of-plane modes from Eqs. (27) and (31), such that

$$\sum_i m_i(1 + 2h_i n_O^2 \xi) \sin 2n_O(\phi_i - \varphi_{n_O}) = 0, \tag{58}$$

$$\sum_i m_i((1 + 2h_i n_O^2 \xi) \cos 2n_O(\phi_i - \varphi_{n_O}) - 2h_i n_O^2 \xi \Lambda_{n_O}) = \sum_i m_i \Xi_i = M\Lambda_{n_O}, \tag{59}$$

where $\Lambda_{n_O} = (\omega_{O2}^2 - \omega_{O1}^2)/(\omega_{O1}^2 + \omega_{O2}^2)$ and it has been assumed that second order products of the radial and axial positions in Eqs. (27) and (31) are negligible. This is reasonable provided that the ring is thin.

To eliminate the frequency splits from a single pair of predominantly in-plane and a single pair of predominantly out-of-plane modes of vibration, the equivalent imperfection masses and their angular positions can be found by solving Eqs. (56)–(59) for m_i, h_i and ϕ_i. These equations can be solved in a number of different ways. For example, the radial or angular positions can be set as variables or pre-determined constants, as could the magnitudes of the masses. As can seen by comparing previous studies [19,20], the simplest analytical solution can be determined by leaving only one variable, the magnitude. In this case, one possible solution to Eqs. (56)–(59) is

$$m_1 = -\sum_{i=2}^{N} m_i \frac{\sin 2n_I(\phi_i - \varphi_{n_I})}{\sin 2n_I(\phi_1 - \varphi_{n_I})}, \quad m_2 = -\sum_{i=3}^{N} m_i \frac{\zeta_{1i}}{\zeta_{12}}, \tag{60, 61}$$

$$m_3 = \frac{M\lambda_{n_I}\zeta_{12} - \sum_{i=4}^{N} m_i\chi_i}{\chi_3}, \quad \sum_{i=4}^{N} m_i\kappa_i = M\tau_\Xi, \tag{62, 63}$$

where ζ_{ij}, χ_i, κ_i and τ_Ξ are constant terms defined in Appendix A (see Eqs. (A.1–A.4)) and N is the total number of trimming masses to be applied to the ring.

As noted in Ref. [20], there are an infinite number of solutions to Eqs. (60)–(63) if the total number of trimming masses is greater than the number of equations to be solved. One possible solution to Eq. (63) for $4 \leqslant i \leqslant N$ is

$$m_i = \frac{M}{(N-3)} \frac{\tau_\Xi}{\kappa_i}. \tag{64}$$

Using Eqs. (60)–(64) the frequency splits and orientations of a single pair of predominantly in-plane modes and a single pair of predominantly out-of-plane modes can be represented equivalently as N imperfection masses attached at predetermined positions to a perfect ring. Performing the inverse procedure, the frequency splits can be eliminated simultaneously by the removal of the same imperfection masses. This procedure will be demonstrated later through numerical example. However, before doing this, elimination of the in-plane/out-of-plane coupling needs to be considered.

3.2. Stage 2. Elimination of the in-plane/out-of-plane coupling

If no coupling exists in the imperfect ring that is to be trimmed, it is a simple process to prevent coupling from entering the system. It can be seen from the off-diagonal coupling terms in Eq. (23), that cross-coupling can be avoided by applying the masses on the central plane of the ring, i.e., at $L_i = 0$. In practice, this can be achieved by dividing each mass in half and applying one half at $L/2$ and the other half at $-L/2$. However, in a typical ring coupling will exist and will need to be eliminated.

To determine the coupling and so eliminate it, it is necessary to consider the amplitudes of the in-plane (Eq. (47)) and the out-of-plane (Eq. (49)) displacements of the ring in response to externally applied forces. These equations need to be solved to ensure that there is a minimum amount of in-plane/out-of-plane coupling.

In a practical device, the coupling will be identified by the application of external forces in either an in-plane or an out-of-plane direction and by comparing the responses of the in-plane and out-of-plane motions. The forces will be applied along specific generalized co-ordinates so as to simplify Eqs. (47)–(50). If a mass lies at a nodal position of the in-plane generalized co-ordinate along which an excitation force is applied, the effect of that mass on the coupling will not be observed and so would appear not to exist. To detect that mass, a second force will need to be applied to the other in-plane generalized co-ordinate. Hence, two forces will need to be applied to ensure that the effects of all of the imperfection masses are observed. Similarly, the motion of the ring in the coupled direction (i.e., the out-of-plane direction if an in-plane force is applied) needs to be measured at two distinct positions just in case the masses lie at nodal positions of the coupled out-of-plane generalized co-ordinates. For these reasons, four combinations of external forces and orthogonal sensor positions are required to fully assess the effect of all of the mass imperfections on the in-plane/out-of-plane coupling. For the following analysis, it will be assumed that in-plane forces will be applied and two combinations of out-of-plane sensor position are required for each in-plane force.

The response of the ring in the in-plane and the out-of-plane directions to a force associated with the first in-plane generalized co-ordinate F_{I1} has already been considered, see Eqs. (51) and (52). A similar pair of equations can be generated for a force F_{I2}. The ratio of the out-of-plane to in-plane motion for applied forces F_{I1} and F_{I2} is

$$\frac{V(F_{I1},\phi_{po})}{W(F_{I1},\phi_{pi})}=\frac{\omega^2}{n_I\cos n_I(\phi_{pi}-\varphi_{n_I})}\left(\begin{array}{l}(B_{I1O1}\cos\Psi_{O1}-B_{I1O2}\cos\Psi_{O2})^2\\ \quad+(B_{I1O1}\sin\Psi_{O1}-B_{I1O2}\sin\Psi_{O2})^2\end{array}\right)^{1/2}, \tag{65}$$

$$\frac{V(F_{I2},\phi_{po})}{W(F_{I2},\phi_{pi})}=\frac{\omega^2}{n_I\sin n_I(\phi_{pi}-\varphi_{n_I})}\left(\begin{array}{l}(B_{I2O1}\cos\Psi_{O1}-B_{I2O2}\cos\Psi_{O2})^2\\ \quad+(B_{I2O1}\sin\Psi_{O1}-B_{I2O2}\sin\Psi_{O2})^2\end{array}\right)^{1/2}, \tag{66}$$

where B_{I1O1} and B_{I2O1} are given by Eq. (54) and B_{I1O2} and B_{I2O2} are given by Eq. (55). These terms depend upon the angular locations of the out-of-plane sensors ϕ_{po}, see Fig. 5. Thus, Eqs. (65) and (66) can be used to generate the four equations that need to be solved to represent the measured out-of-plane/in-plane coupling V/W, as determined by in-plane and out-of-plane sensors at angular positions of ϕ_{pi} and ϕ_{po}, respectively, as a set of equivalent imperfection masses. Once these imperfection masses have been calculated, their removal will eliminate the coupling. A general solution and a more specific solution to the problem of calculating the equivalent imperfection masses will be outlined next.

(i) *The general solution*: The magnitude, angular positions and radial positions of the trimming masses were determined in Section 3.1. Consequently, only the axial positions of these trimming masses need to be considered here. A general solution can be determined by finding the minimum of

$$\sum_{\phi_{po}}\left(1-\frac{W(F_{I1},\phi_{pi})}{V(F_{I1},\phi_{po})}\frac{\omega^2}{n_I\cos n_I(\phi_{pi}-\varphi_{n_I})}\left(\begin{array}{l}(B_{I1O1}\cos\Psi_{O1}-B_{I1O2}\cos\Psi_{O2})^2\\ \quad+(B_{I1O1}\sin\Psi_{O1}-B_{I1O2}\sin\Psi_{O2})^2\end{array}\right)^{1/2}\right)^2$$
$$+\sum_{\phi_{po}}\left(1-\frac{W(F_{I2},\phi_{pi})}{V(F_{I2},\phi_{po})}\frac{\omega^2}{n_I\sin n_I(\phi_{pi}-\varphi_{n_I})}\left(\begin{array}{l}(B_{I2O1}\cos\Psi_{O1}-B_{I2O2}\cos\Psi_{O2})^2\\ \quad+(B_{I2O1}\sin\Psi_{O1}-B_{I2O2}\sin\Psi_{O2})^2\end{array}\right)^{1/2}\right)^2, \tag{67}$$

where the summation is over the out-of-plane sensors. The in-plane and out-of-plane displacements, $W(F_k,\phi_{pi})$ and $V(F_k,\phi_{po})$, are measured at two distinct out-of-plane angular positions of ϕ_{po} and $\phi_{po}+\pi/2n_O$. The second angle has been chosen because the angle between the out-of-plane generalized co-ordinates is $\pi/2n_O$.

The only variables in Eq. (67) are the axial positions of the masses and these terms appear as linear contributions in the B_k terms. In general, the minimum of Eq. (67) can be solved either graphically or by using numerical search techniques. However, for a practical arrangement of a sensor, it is possible to obtain an algebraic solution, as discussed next.

(ii) *An algebraic solution*: It is possible to obtain an algebraic solution to Eq. (67) when the out-of-plane generalized co-ordinates and the out-of-plane sensors are aligned ($\phi_{po}=\varphi_{n_O}$). In this case, an individual out-of-plane sensor will only measure the displacement along a single out-of-plane generalized co-ordinate, significantly simplifying Eqs. (65) and (66).

Before considering this simplification method in detail, it is worthwhile noting that two different methods can be used to align the out-of-plane generalized co-ordinates and the out-of-plane sensors. By introducing deliberate imperfections into the structure of the ring, the modes can be aligned at, or close to, a particular angular position. Analysis of a method for doing this is briefly described in Appendix I of [20]. This method would have to be used if the angular positions of the sensors are fixed by the manufacturing process with respect to the physical structure of the ring, for example by being etched onto the surface. If the manufacturing process does not fix the angular positions of the sensors, the alignment of the generalized co-ordinates and the sensors can be achieved easily by simply rotating the ring until the correct alignment is achieved. The prototype ring and sensor structure designed by Eley [2] can be aligned in this way.

Whichever method is used to align the out-of-plane generalized co-ordinates and sensors, the ratio of the out-of-plane displacements to in-plane displacements measured by the two sensors in response to in-plane forces of F_{I1} and F_{I2} can be determined from Eqs. (65) and (66), by substituting $\phi_{po} = \varphi_{n_O}$ and $\phi_{po} = \varphi_{n_O} + \pi/2n_O$. Since the mass terms m_k involve a linear summation (see Eqs. (12)–(15)), Eqs. (65) and (66) can be rewritten in the form of four linear equations as

$$\sum_i G_k(m_i)L_i = \vartheta_k, \tag{68}$$

where $k = I1O1$, $I1O2$, $I2O1$ and $I2O2$ and G_k and ϑ_k are defined in Appendix A (see Eqs. (A.5)–(A.12)).

In a similar manner to that described in Section 3.1, when determining the magnitudes of the trimming masses from Eqs. (56)–(59), there are an infinite number of solutions that can be obtained from Eq. (68) and one possible solution set is

$$L_1 = \frac{\vartheta_{I1O1} - \sum_{i=2}^{N} L_i G_{I1O1}(m_i)}{G_{I1O1}(m_1)}, \tag{69}$$

$$L_2 = \frac{(\vartheta_{I1O2}G_{I1O1}(m_1) - \vartheta_{I1O1}G_{I1O2}(m_1)) - \sum_{i=3}^{N} L_i(G_{I1O1}(m_1)G_{I1O2}(m_i) - G_{I1O1}(m_i)G_{I1O2}(m_1))}{(G_{I1O1}(m_1)G_{I1O2}(m_2) - G_{I1O1}(m_2)G_{I1O2}(m_1))}, \tag{70}$$

$$L_3 = \frac{\vartheta_1 - \sum_{i=4}^{N} L_i G_1(m_i)}{G_1(m_3)}, \tag{71}$$

$$\sum_{i=4}^{N} L_i(G_1(m_3)G_2(m_i) - G_2(m_3)G_1(m_i)) = \vartheta_2 G_1(m_3) - \vartheta_1 G_2(m_3), \tag{72}$$

where G_1, G_2, ϑ_1 and ϑ_2 are defined in Appendix A (see Eqs. (A.13) and (A.14)).

Similarly, if the number of trimming masses N is greater than 4, there are an infinite number of solutions to Eq. (72), one of which is that for $4 \leqslant i \leqslant N$ is

$$L_i = \frac{\vartheta_2 G_1(m_3) - \vartheta_1 G_2(m_3)}{(N-3)(G_1(m_3)G_2(m_i) - G_2(m_3)G_1(m_i))}. \tag{73}$$

In summary, if the out-of-plane displacement of the ring can be measured by a pair of out-of-plane sensors that are aligned with the out-of-plane generalized co-ordinates, the in-plane/out-of-plane coupling can be represented "equivalently" by positioning the imperfection masses at the axial positions given by Eqs. (69)–(73). Inversely, by removing the trimming masses from these positions, the in-plane/out-of-plane coupling can be eliminated from the system. This will be demonstrated later using a numerical example.

3.3. Stage 3. Matching the in-plane and out-of-plane natural frequencies

In the analysis performed so far, the elimination of the frequency splits and the in-plane/out-of-plane coupling has been produced by the use of trimming masses. A similar method can also be applied to eliminate the difference between the in-plane and out-of-plane natural frequencies. Assuming that the frequency splits of the in-plane and out-of-plane modes have been eliminated successfully, it is a simple task to use Eqs. (26) and (27) to determine the trimmed natural frequencies resulting from Stage 1. These are given by

$$\omega_{0I}^2 = \frac{2M\omega_{I1}^2\omega_{I2}^2}{(M-\sum_i m_i)(\omega_{I1}^2+\omega_{I2}^2)}, \quad \omega_{0O}^2 = \frac{2(M+2n_O^2\xi\sum_i m_i h_i)\omega_{O1}^2\omega_{O2}^2}{(M-\sum_i m_i)(\omega_{O1}^2+\omega_{O2}^2)}. \tag{74, 75}$$

Comparing these equations it can be seen that the in-plane and out-of-plane natural frequencies could have been trimmed to the same perfect natural frequency by carefully selecting the radial positions h_i of the trimming masses. Letting $\omega_{0I} = \omega_{0O}$ and combining Eqs. (74) and (75) indicates that this is achieved if

$$\sum_i m_i h_i = \frac{M}{2n_O^2\xi}\left(\frac{\omega_{I1}^2\omega_{I2}^2}{\omega_{O1}^2\omega_{O2}^2}\frac{(\omega_{O1}^2+\omega_{O2}^2)}{(\omega_{I1}^2+\omega_{I2}^2)}-1\right). \tag{76}$$

If the radial positions of the trimming masses had not been considered to be constant in Section 3.1, the natural frequencies of the predominantly in-plane and predominantly out-of-plane modes could have been deliberately trimmed to the same frequency by simultaneously solving Eqs. (56)–(59) and (76). The reason why this was not proposed earlier was because of the practical constraint that mass can only be added or removed from the surface of the ring. Previously, it was necessary to have the axial positions of the trimming masses as being variable to allow the in-plane/out-of-plane coupling to be eliminated. To achieve this in practice, the trimming masses will need to be applied in pairs on opposite faces of the ring at particular angular positions to replicate the addition of a single trimming mass inside the ring. Allowing the radial position to be variable as well, the pair of trimming masses will need to be split into a set of four trimming masses applied at the four corners of the cross-section of the ring. This increases the complexity of the trimming process and increases the possibility of errors entering the trimming process.

Another reason for not matching the natural frequencies earlier was due to a consideration of the effect of errors in the trimming process. If the trimming masses are not applied in the correct proportions at the correct locations, errors will be introduced into the system, which have the potential to increase the in-plane/out-of-plane coupling. If the natural frequencies of the predominantly in-plane and out-of-plane modes are sufficiently far apart, this coupling can be compensated for easily. However, if the natural frequencies are close together, the modes may become complex combinations of in-plane and out-of-plane contributions and it will be more

difficult to compensate for the errors. For this reason, it is preferable that ω_{0I} and ω_{0O} are not close together.

The matching of the in-plane and out-of-plane natural frequencies for a pair of unsplit frequencies and no in-plane/out-of-plane coupling will now be outlined. As before, the trimming will be performed by the application of trimming masses and so a modified set of the equations used in Sections 3.1 and 3.2 will be used here. It is necessary to consider the effect that the trimming masses will have on the natural frequencies and in-plane/out-of-plane coupling so that a set of masses can be chosen that introduce no frequency splits and no in-plane/out-of-plane coupling.

For example consider Eqs. (56)–(59), which are used to trim the natural frequencies of the in-plane and out-of-plane modes in Stage 1. Setting $\omega_{I1} = \omega_{I2}$ and $\omega_{O1} = \omega_{O2}$ in these equations gives

$$\sum_i m_i \sin 2n_I(\phi_i - \varphi_{n_I}) = 0, \quad \sum_i m_i \cos 2n_I(\phi_i - \varphi_{n_I}) = 0, \tag{77, 78}$$

$$\sum_i m_i(1 + 2h_i n_O^2 \xi) \sin 2n_O(\phi_i - \varphi_{n_O}) = 0,$$

$$\sum_i m_i(1 + 2h_i n_O^2 \xi) \cos 2n_O(\phi_i - \varphi_{n_O}) = 0. \tag{79, 80}$$

The aim of the trimming process is to eliminate the difference between the in-plane and out-of-plane natural frequencies without introducing frequency splits into either the in-plane or the out-of-plane modes. This is achieved if Eqs. (77)–(80) are satisfied. The problem of determining such solutions is immediately simplified by applying trimming masses of identical magnitude at each angular position and by fixing the angular positions of the trimming masses in a simple pattern, such as by having uniformly spaced trimming masses. For such an arrangement of masses, it is important to realise that certain numbers of uniformly spaced trimming masses (N) can introduce frequency splits into either the in-plane or out-of-plane modes and/or in-plane/out-of-plane coupling.

Consider a set of N masses of equal magnitude, placed at the same radial distance from the centre-line of the ring and positioned at regular intervals around the circumference of the ring, such that the angular separation between neighbouring masses is $2\pi/N$, see Fig. 7. It can be shown [23] for this configuration that Eqs. (77)–(80) can only be satisfied if $2n_I/N$ is not an integer and $2n_O/N$ is not an integer.

Consider next the influence of the masses on the in-plane/out-of-plane coupling. By rearranging Eq. (68) it can be shown that there will be no in-plane/out-of-plane coupling introduced to the ring provided that

$$\sum_i m_i L_i(\cos(n_O + n_I)\phi_i \pm \cos(n_O - n_I)\phi_i) = 0, \tag{81}$$

$$\sum_i m_i L_i(\sin(n_O + n_I)\phi_i \pm \sin(n_O - n_I)\phi_i) = 0. \tag{82}$$

There are a number of possible solutions to these equations. A trivial solution exists when L_i is equal to zero for each mass, i.e., each mass lies on the central plane of the ring. Alternatively, if L_i

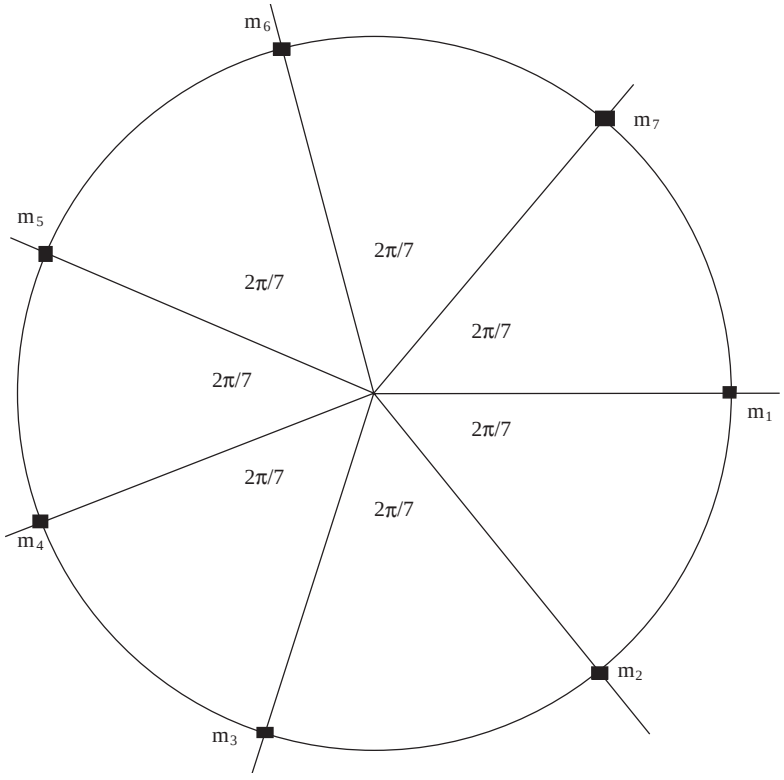

Fig. 7. Angular positions of $N = 7$ uniformly spaced trimming masses.

is a non-zero constant, it can be shown that no coupling exists when N is not equal to $(n_O + n_I)$, $2(n_O + n_I)$, $(n_O - n_I)$ or $2(n_O - n_I)$—assuming that the masses are identical and uniformly spaced.

So far it has been shown that it is possible to use a set of regularly spaced trimming masses to modify the natural frequencies of the in-plane and out-of-plane modes of vibration without introducing either frequency splits and/or in-plane/out-of-plane coupling. To determine the trimming masses required to match the in-plane and out-of-plane natural frequencies, it is necessary to consider the frequency that the modes are to be trimmed to by the second set of trimming masses. The natural frequencies that the in-plane and out-of-plane modes are trimmed to are given by Eqs. (74) and (75), respectively, where $\omega_{I1} = \omega_{I2}$ and $\omega_{O1} = \omega_{O2}$ are taken to be the natural frequencies of the ring after Stage 1. Eq. (76) provides the relationship between the in-plane and out-of-plane natural frequencies (after Stage 1), the second set of trimming masses and their radial positions. Fixing the radial positions of the trimming masses, and setting the natural frequencies after the first trimming process to be ω_{I1} and ω_{O1}, the required magnitude of each of the second set of N trimming masses can be shown to be

$$m_i = \frac{M}{2n_O^2 h_i N \xi}\left(\frac{\omega_{I1}^2}{\omega_{O1}^2} - 1\right). \tag{83}$$

The value of h_i has been fixed at the same value for each mass, although no value has been specified. Values for h_i will be considered now. The initial difference between the in-plane and

out-of-plane natural frequencies will be significant in the choice of radial positions. If $\omega_{I1} < \omega_{O1}$, a positive value for h_i would indicate that imperfection masses had been removed from the ring and so require that the trimming masses are added to the ring, whilst a negative value would indicate that imperfection masses had been added to the ring and so require that the trimming masses are removed from the ring. Similarly, if $\omega_{I1} > \omega_{O1}$, a positive value for h_i would require that the trimming masses are removed from the ring whilst a negative value would require that the trimming masses are added to the ring.

In summary, a method for trimming the two in-plane and the two out-of-plane modes of vibration to identical natural frequencies has been devised. The proposed method will be demonstrated in the numerical examples that follow.

4. Numerical examples

Numerical examples will be used to verify the solutions to the proposed trimming methods described in Section 3 and will be performed in three stages. In Stage 1, Eqs. (60)–(63) will be solved to determine the magnitude and radial positions of the trimming masses needed to eliminate the frequency splits from a pair of predominantly in-plane modes and a pair of predominantly out-of-plane modes. In Stage 2, Eqs. (69)–(72) are solved to determine the axial positions of the trimming masses arising from Stage 1 to eliminate the in-plane/out-of-plane coupling. In Stage 3, Eq. (83) is used to determine the second set of N trimming masses, to match the in-plane and out-of-plane natural frequencies. At each stage of the trimming process, the natural frequencies and orientations of the four modes are calculated.

As in the earlier numerical example, the dimensions of the ring are taken to be $\rho = 8250\ \text{kg/m}^3$, $R = 0.0415$ m, $h = 0.003$ m and $L = 0.00105$ m and it is assumed to be initially perfect with the unsplit in-plane 2ϕ modes having a natural frequency of 4000 Hz and the unsplit out-of-plane 3ϕ modes having a natural frequency of 4004 Hz. Applying two imperfection masses of 0.05% and 0.1% of the mass of the perfect ring M_0 at 0° and 35°, respectively, with each mass applied at a corner with $h_i = -h/2$ and $L_i = L/2$, the in-plane and out-of-plane natural frequencies split. The resulting in-plane modes have frequencies of 3997.837 and 3996.171 Hz with the higher frequency mode orientated at -16.88°. The resulting out-of-plane modes have frequencies of 4002.648 and 4000.746 Hz with the lower frequency mode orientated at 8.97°. Throughout all stages of the trimming process the N trimming masses are uniformly spaced around the circumference of the ring and in the tabulated data the angular position of one mass, such as ϕ_2, can be found by adding $2\pi/N$ onto the angular position of the previous mass, ϕ_1. The number of trimming masses is chosen such that $N = 7$ (see Fig. 7)—this choice of N ensures that identical, uniformly spaced masses do not split the in-plane 2ϕ modes and the out-of-plane 3ϕ modes.

4.1. Stage 1. Elimination of the frequency splits from a pair of predominantly in-plane modes and a pair of predominantly out-of-plane modes

Each row of Tables 1 and 2 shows results for the magnitude of the ($N = 7$) uniformly spaced trimming masses required to perform Stage 1 of the trimming procedure. The trimming masses indicated in Table 1 have been determined by fixing the radial position h_i of each of the trimming

Table 1
Simultaneous elimination of the frequency splits from a pair of in-plane and a pair of out-of-plane modes with $h_i = -h/2$ for all trimming masses

ϕ_1 (rad)	m_1/M (%) L_1 (mm)	m_2/M (%) L_2 (mm)	m_3/M (%) L_3 (mm)	m_4/M (%) L_4 (mm)	m_5/M (%) L_5 (mm)	m_6/M (%) L_6 (mm)	m_7/M (%) L_7 (mm)	ω_{0I} (Hz)	ω_{0O} (Hz)	ω_{0I}/ω_{0O}
0	0.033	−0.008	−0.046	0.007	−0.012	0.012	−0.007	3997.4	4002.0	0.9989
	−1.215	2.311	0.788	1.543	−1.068	−1.068	1.543			
$2\pi/7$	0.005	−0.047	−0.020	−0.014	0.025	−0.025	0.014	3998.2	4002.7	0.9989
	−3.344	0.472	−1.473	−0.914	0.632	0.633	−0.914			
$4\pi/7$	−0.052	−0.009	−0.021	0.011	−0.019	0.019	−0.011	3998.6	4003.0	0.9989
	0.015	−2.478	−2.136	0.680	−0.471	−0.471	0.680			
$6\pi/7$	−0.019	−0.035	0.057	0.004	−0.008	0.008	−0.004	3996.9	4001.7	0.9988
	−2.037	−0.987	0.473	0.502	−0.348	−0.347	0.502			
$8\pi/7$	−0.038	0.051	0.021	0.001	−0.002	0.002	−0.001	3996.3	4001.2	0.9988
	−1.571	−0.079	0.860	−7.312	5.061	5.060	−7.313			
$10\pi/7$	0.041	0.015	0.034	0.009	−0.015	0.015	−0.009	3995.2	4000.3	0.9987
	0.175	−0.831	−0.543	−2.045	1.415	1.415	−2.045			
$12\pi/7$	0.031	0.032	−0.024	−0.017	0.031	−0.031	0.017	3996.2	4001.1	0.9988
	−1.597	0.030	2.584	0.365	−0.253	−0.253	0.365			
0	0.056	−0.011	−0.054	0.028	0	0	0	3996.6	4001.4	0.9988
	−0.914	−1.080	1.097	1.543						
0	0.007	−0.039	−0.042	0	−0.050	0	0	3999.5	4003.6	0.9990
	0.233	0.776	−0.408		−1.067					
0	0.029	0.023	−0.020	0	0	0.050	0	3995.4	4000.4	0.9987
	−3.268	−0.289	3.945			−1.068				
0	0.041	−0.005	−0.070	0	0	0	−0.028	3998.2	4002.6	0.9989
	−0.424	10.754	0.365				1.543			

masses at $-h/2$. The trimming masses shown in Table 2 have been determined by fixing the radial position of each of the odd-numbered trimming masses at $-h/2$ and of each of the even-numbered trimming masses at $h/2$. The trimming masses are presented as a percentage of the mass of the original perfect ring. The trimming masses shown successfully eliminate the frequency splits of the pair of predominantly in-plane and out-of-plane modes to the frequencies shown.

It can be seen from Table 1 that the modes can be trimmed simultaneously to a variety of different frequencies—the results shown are obtained by varying the order in which the angular positions are substituted into the relevant equations. In addition, comparing Tables 1 and 2 it can be seen that varying the radial position of the trimming masses produce different sets of trimming masses and trim the modes to different natural frequencies. Depending on the choice of radial positions and the choice of the order in which the trimming masses are considered, it is possible to vary the natural frequencies that the modes are trimmed to and it may be possible to trim the modes to frequencies that are closer together or further apart than the initial splits. It can be seen from the final columns of Tables 1 and 2 that the ratio of the trimmed in-plane natural frequency to the trimmed out-of-plane natural frequency does not have a fixed value, although the variation in the ratio is small for the trimming masses shown.

Table 2
Simultaneous elimination of the frequency splits from a pair of in-plane and a pair of out-of-plane modes with $h_i = -h/2$ for all odd-numbered trimming masses and $h_i = h/2$ for all even-numbered trimming masses

ϕ_1 (rad)	m_1/M (%) L_1 (mm)	m_2/M (%) L_2 (mm)	m_3/M (%) L_3 (mm)	m_4/M (%) L_4 (mm)	m_5/M (%) L_5 (mm)	m_6/M (%) L_6 (mm)	m_7/M (%) L_7 (mm)	ω_{0I} (Hz)	ω_{0O} (Hz)	ω_{0I}/ω_{0O}
0	0.034	−0.0005	−0.041	0.006	−0.012	0.015	−0.007	3997.1	4001.6	0.9989
	−1.174	38.617	0.893	1.917	−1.068	−0.860	1.543			
$2\pi/7$	0.011	−0.046	−0.022	−0.011	0.025	−0.032	0.014	3998.2	4003.4	0.9987
	−1.360	0.484	−1.333	−1.136	0.632	0.510	−0.914			
$4\pi/7$	−0.051	0.002	−0.013	0.009	−0.019	0.024	−0.011	3998.2	4002.3	0.9990
	0.015	12.575	−3.495	0.845	−0.471	−0.379	0.680			
$6\pi/7$	−0.014	−0.022	0.064	0.003	−0.008	0.009	−0.004	3996.4	4001.3	0.9988
	−2.767	−1.528	0.417	0.624	−0.347	−0.280	0.502			
$8\pi/7$	−0.046	0.039	0.014	0.001	−0.002	0.003	−0.001	3996.8	4001.2	0.9989
	−1.316	−0.104	1.258	−9.093	5.065	4.081	−7.319			
$10\pi/7$	0.039	0.018	0.037	0.007	−0.015	0.019	−0.009	3995.1	3999.8	0.9988
	0.185	−0.704	−0.496	−2.541	1.415	1.410	−2.045			
$12\pi/7$	0.026	0.010	−0.040	−0.014	0.031	−0.039	0.017	3997.2	4002.2	0.9987
	−1.886	0.094	1.574	0.454	−0.253	−0.204	0.365			
0	0.062	−0.007	−0.058	0.022	0	0	0	3996.6	4001.3	0.9988
	−0.831	−1.847	1.021	1.917						
0	0.012	−0.029	−0.036	0	−0.050	0	0	3999.1	4003.5	0.9989
	0.126	1.048	−0.471		−1.068					
0	0.022	0.037	−0.0001	0	0	0.062	0	3994.6	3999.0	0.9989
	−4.359	−0.179	650.6			−0.860				
0	0.042	−0.003	−0.069 0	0	0	0	−0.028	3998.2	4002.6	0.9989
	−0.417	14.520	0.369				1.543			

4.2. Stage 2. Elimination of the in-plane/out-of-plane coupling

Tables 1 and 2 also include the axial positions of the required trimming masses to eliminate the in-plane/out-of-plane coupling. To determine the coupling, the in-plane sensor is aligned for all four equations at $\phi_{pi} = \varphi_{no}$, which is a valid position for the sensor as it is not a nodal position for either of the in-plane generalized co-ordinates. The coupling is calculated using the original imperfection masses using Eqs. (65) and (66), and the axial positions are calculated using Eqs. (69)–(73). For clarity, the axial positions shown in Tables 1 and 2 have been recorded in millimetres and should be compared with the axial distance from the centre of the ring to its upper and lower surfaces, which is 0.525 mm.

In principle, if the trimming masses are placed at these axial positions, the in-plane/out-of-plane coupling is eliminated from all four modes of vibration, leaving a pair of purely in-plane modes and a pair of purely out-of-plane modes. The applicability of the presented axial positions are limited because they do not lie on the surface of the ring. It can be noted that most of the axial positions are outside the cross-section of the ring and many of them are at a significant distance

from the surface. For this practical reason, it is necessary to modify the axial positions of the trimming masses.

There are three possible methods of modifying the axial positions: (i) the individual trimming masses can be split into two masses and applied on opposite faces of the ring; (ii) larger trimming masses can be calculated using a modified form of Eqs. (63) and (64); (iii) the axial positions can be adjusted by modifying Eqs. (69)–(73). Each of these methods are considered next.

(i) *Division of the trimming masses into pairs of trimming masses*: Dividing the trimming masses into pairs of trimming masses is possible because the in-plane/out-of-plane coupling is linearly dependent on the axial position L_i of the masses, and the natural frequencies of the predominantly out-of-plane modes are approximately linearly dependent on the radial positions of the masses. Thus, if a trimming mass m_i is required to be removed from inside the ring (for example at $-L/2<L_i<L/2$), the same effect can be achieved by applying two masses on opposite faces of the cross-section of the ring (at $\pm L/2$) with the size of the two masses, m_{i+} and m_{i-}, given by

$$\frac{m_{i+}L}{2}-\frac{m_{i-}L}{2}=m_iL_i \quad \text{and} \quad m_{i+}+m_{i-}=m_i. \tag{84,85}$$

Consider the effect of doing this for the example considered. Table 3 records the magnitude of the 14 trimming masses that would result from applying Eqs. (84) and (85) to the trimming masses of Table 1. m_{i+} and m_{i-} indicate the masses that would be applied at axial positions of $L/2$ and $-L/2$, respectively at angular position ϕ_i. Comparing Tables 1 and 3, it can be seen, as expected, that the effective trimming mass applied at each angular position has not increased, although the overall magnitude of the two trimming masses may be larger than the original mass if the original mass was to be placed outside of the cross-section of the ring.

The trimming masses shown in Table 3 can be used in a practical process to simultaneously eliminate the frequency splits of the predominantly in-plane and out-of-plane modes and the in-plane/out-of-plane coupling. This is demonstrated in Fig. 8, which has been formed by applying the two imperfection masses and the last set of trimming masses recorded in Table 3 (the set with the 0.004% and 0.037% masses applied at 0 radians) incrementally to the perfect ring and calculating the natural frequencies and mode shapes at each stage. This was done to investigate how far the mode shapes deviate from being purely in-plane and out-of-plane as the original imperfection masses are added to the perfect ring and then how closely the trimming masses return the modes to being purely in-plane or out-of-plane. For continuity, in Fig. 8 both stages have been shown in the same graph. In Fig. 9, this will be taken one stage further to include the trimming of the in-plane and out-of-plane modes to the same natural frequency.

Fig. 8 consists of five separate figures. Figs. 8(a)–(d) represent the eigenvectors. The proportion of the mode shape along the two in-plane and two out-of-plane generalized co-ordinates is represented in the four curves. In each of Figs. 8(a)–(d), only three of the four generalized co-ordinates can be seen due to the vertical scale. The displacement of the fourth generalized co-ordinate, at approximately unity, is significantly larger than those of the other three generalized co-ordinates and indicates the predominant contribution to each mode. For each mode, the sum of the square of the displacements along each generalized co-ordinate at a specific frequency is equal to unity.

Fig. 8(e) shows the natural frequencies of the four modes shown in Figs. 8(a)–(d). It can be seen that there are two sets of curves in Fig. 8(e); one solid, one dashed. The two sets have been

Table 3
Simultaneous elimination of the frequency splits from a pair of in-plane and a pair of out-of-plane modes with $h_i = -h/2$ for all trimming masses

ϕ_1 (rad)	m_{1+}/M (%)	m_{2+}/M (%)	m_{3+}/M (%)	m_{4+}/M (%)	m_{5+}/M (%)	m_{6+}/M (%)	m_{7+}/M (%)
	m_{1-}/M (%)	M_{2-}/M (%)	M_{3-}/M (%)	M_{4-}/M (%)	M_{5-}/M (%)	M_{6-}/M (%)	M_{7-}/M (%)
0	−0.022	−0.022	−0.058	0.014	0.006	−0.006	−0.014
	0.055	0.014	0.012	−0.007	−0.019	0.017	0.007
$2\pi/7$	−0.012	−0.045	0.018	0.005	0.028	−0.028	−0.005
	0.017	−0.002	−0.038	0.017	−0.003	0.003	0.019
$4\pi/7$	−0.027	0.017	0.032	0.012	−0.001	0.001	−0.012
	−0.026	−0.026	−0.052	−0.002	−0.019	−0.018	0.002
$6\pi/7$	0.027	0.015	0.054	0.004	−0.001	0.001	−0.004
	−0.046	−0.050	0.003	0.00009	−0.006	0.006	−0.00009
$8\pi/7$	0.038	0.022	0.028	−0.008	−0.012	0.012	0.008
	−0.076	0.030	−0.007	0.009	0.010	−0.010	−0.009
$10\pi/7$	0.027	−0.004	−0.0006	−0.012	−0.028	0.028	0.012
	0.014	0.020	0.034	0.021	0.013	−0.013	−0.021
$12\pi/7$	−0.031	0.017	−0.072	−0.015	0.008	−0.008	0.015
	0.062	0.015	0.048	−0.003	0.023	−0.023	0.003
0	−0.021	0.006	−0.084	0.054	0	0	0
	0.077	−0.017	0.030	−0.027			
0	0.005	−0.048	−0.005	0	0.026	0	0
	0.002	0.009	−0.037		−0.075		
0	−0.075	0.005	−0.085	0	0	−0.026	0
	0.104	0.018	0.065			0.075	
0	0.004	−0.049	−0.059	0	0	0	−0.054
	0.037	0.045	−0.011				0.027

included to demonstrate the validity of neglecting the terms involving h_i^2 and L_i^2 from the calculations of the out-of-plane natural frequencies (see Eqs. (27) and (31)). The dashed curves are the approximate solutions, whilst the solid curves are the exact solutions. There is a small difference in the results, the exact solution has a slightly lower frequency, but over the entire trimming procedure it can be seen that the difference has a negligible effect. For this reason, it is reasonable to neglect terms involving h_i^2 and L_i^2 in Eqs. (27) and (31).

In the first half of each of the Figs. 8(a)–(e), the magnitude of the imperfection masses applied to the ring increases from 0% to 100% with no trimming masses applied at any point. The ratio of the two imperfection masses is constant throughout. It can be seen from Figs. 8(a)–(d) that as the size of the imperfection masses increases, the size of the in-plane/out-of-plane coupling of each mode increases and, from Fig. 8(e), that the frequency splits of the predominantly in-plane and out-of-plane modes increase.

In the second half of Figs. 8(a)–(e), the magnitude of the trimming masses applied to the ring increases from 0% to 100% with the imperfection masses applied at every point. The ratio of the eight trimming masses is constant throughout. It can be seen that as the size of the trimming masses increase, the size of the in-plane/out-of-plane coupling decreases and the frequency splits

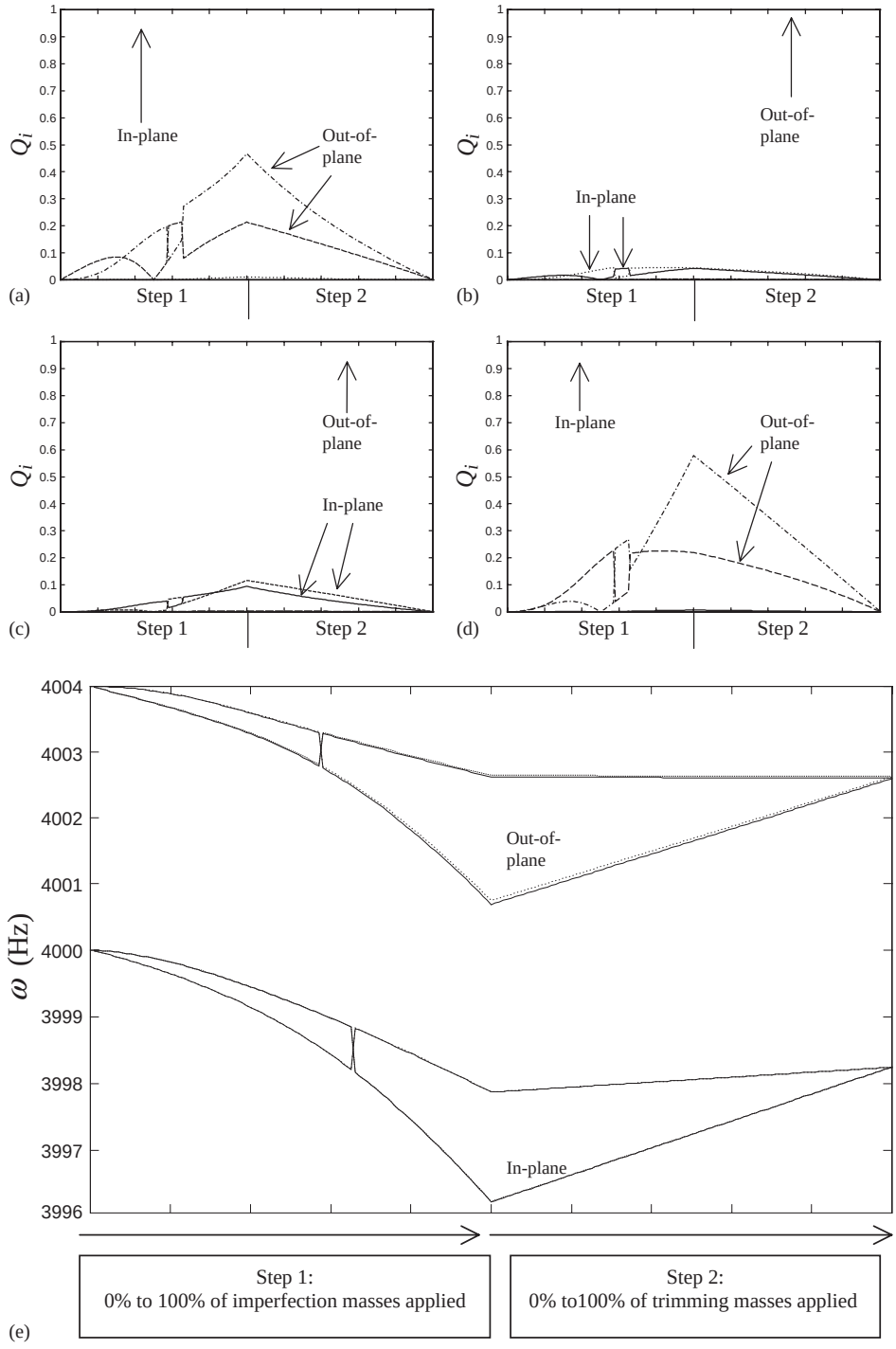

Fig. 8. (a)–(d) In-plane and out-of-plane displacements of the in-plane and out-of-plane modes under trimming using the last trimming masses in Table 3. (e) Natural frequencies of the (predominantly) in-plane and out-of-plane modes of vibration under trimming using the last trimming masses in Table 3.

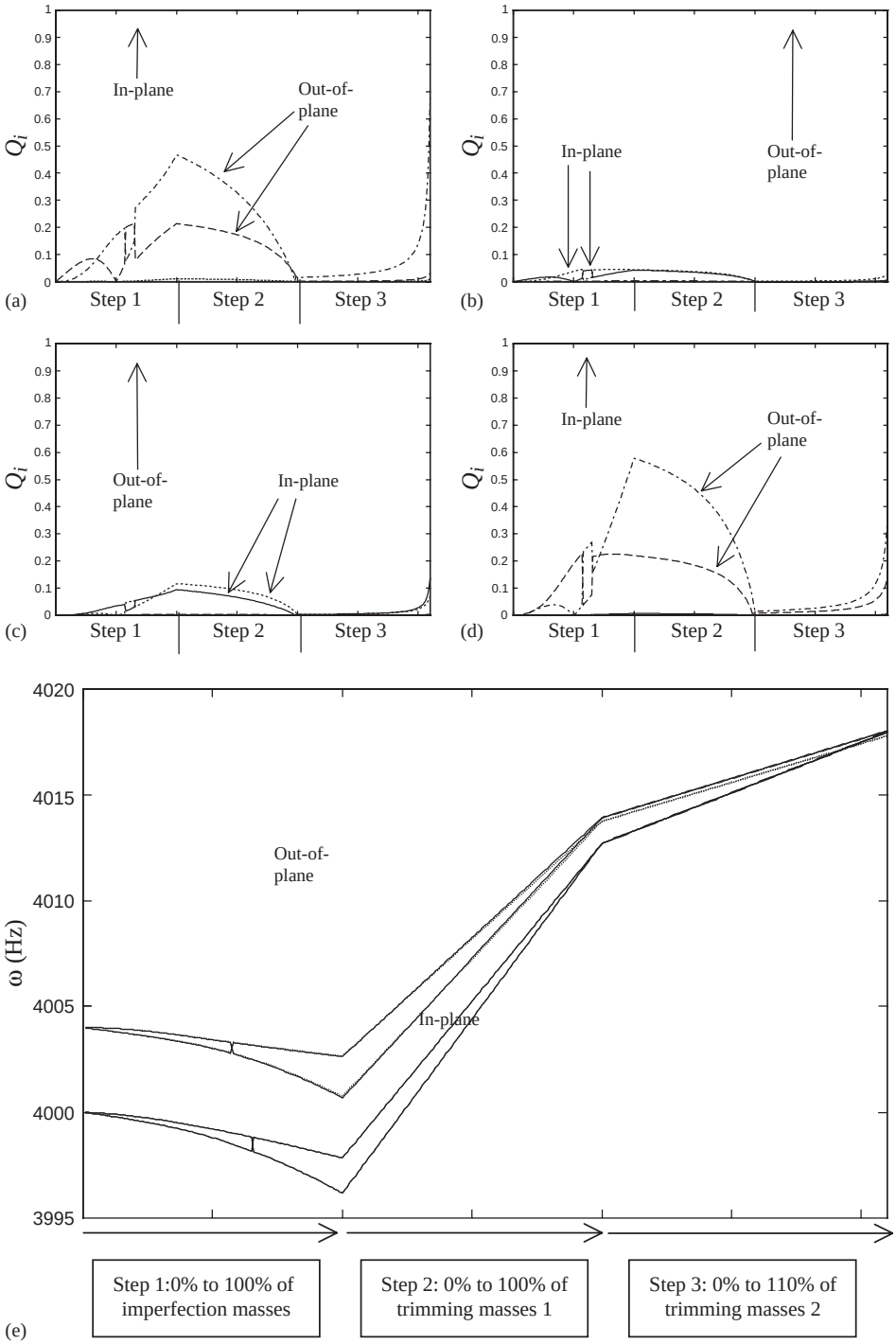

Fig. 9. (a)–(d) In-plane and out-of-plane displacements of the in-plane and out-of-plane modes under trimming using the second set of trimming masses in Table 4. (e) Natural frequencies of the (predominantly) in-plane and out-of-plane modes of vibration under trimming using the second set of trimming masses in Table 4.

also decrease. Thus, the process of eliminating the effect of imperfections from a pair of predominantly in-plane and out-of-plane modes has been demonstrated.

(ii) *Modification of the magnitudes of the trimming masses* (*Eqs.* (60)–(64)): For situations when the calculated trimming mass is located outside of the cross-section of the ring, splitting the trimming mass into a pair of trimming masses will yield one mass that needs to be added to the ring and one that needs to be removed from the ring. This can be problematic if the trimming process is only capable of adding or removing mass. This problem can be solved by considering the magnitude of the trimming masses.

One reason that the trimming masses need to be placed outside the cross-section of the ring is that the trimming masses are small in comparison with the original imperfection masses. Consider Table 1 and specifically the last set of trimming masses (last row), which were used to produce Fig. 8. The largest trimming masses (0.041% and −0.070%) are comparable in size to the two imperfection masses, and these masses are located within the cross-section of the ring. The other two trimming masses are smaller and are located outside of the ring. Indeed, one mass is significantly smaller than the other masses and this is located at a significant distance from the surface of the ring. Thus, it can be seen that smaller masses need to be placed at greater distances from the centre of the ring to satisfy Eqs. (69)–(73).

Thus, if the trimming process can only accommodate the addition or the removal of mass, it is necessary to increase the magnitude of each of the trimming masses. This can be achieved by modifying Eqs. (64) for masses m_i and m_j, where $4 \leqslant i, j \leqslant N$, such that

$$m_i = \frac{(M-a)}{(N-3)}\frac{\tau_\Xi}{\kappa_i} \quad \text{and} \quad m_j = \frac{(M+a)}{(N-3)}\frac{\tau_\Xi}{\kappa_j}, \tag{86, 87}$$

where a is a constant value that is independent of the properties of the ring and the trimming masses and $i \neq j$. This modification can be used to produce larger or smaller trimming masses and has been used previously [20] to produce trimming masses that are all of the same sign.

For example consider Table 4. The first seven solutions in Table 4 have been formed from Table 1 by setting $a = 0.005$, $i = 4$ and 7 and $j = 5$ and 6 in Eqs. (86) and (87). The remaining three solutions have been generated by nullifying masses 4 and 7, replacing the 3 in Eqs. (86) and (87) by 5, setting $i = 6$, $j = 5$ and, in turn, $a = 0.005$, 0.006 and 0.007. Comparing Tables 1 and 4, it can be seen that the magnitude of the trimming masses has increased and that the axial positions have, in general, decreased. Indeed, most of the trimming masses now occur within the cross-section of the ring. There are some exceptions but these are to be expected as the choices of the masses to modify and the values of a were arbitrary.

The final three sets of trimming masses have been included for two reasons. Firstly, to illustrate that as the value of a increases, the size of all the trimming masses may increase, whilst the axial distances of all the trimming masses from the centre-line of the cross-section of the ring will decrease, which has a significant effect on the natural frequencies. Considering the in-plane and out-of-plane natural frequencies, it can be seen that the difference between them increases as a increases, which means that larger trimming masses will be required to match the in-plane and out-of-plane natural frequencies. This can be compensated for by choosing different radial positions for the original set of trimming masses. In each of the three sets shown, the angular position of mass m_1 was 0 radians.

Table 4
Simultaneous elimination of the frequency splits from a pair of in-plane and a pair of out-of-plane modes with $h_i = -h/2$ for all trimming masses

ϕ_1 (rad)	m_1/M (%) L_1 (mm)	m_2/M (%) L_2 (mm)	m_3/M (%) L_3 (mm)	m_4/M (%) L_4 (mm)	m_5/M (%) L_5 (mm)	m_6/M (%) L_6 (mm)	m_7/M (%) L_7 (mm)	ω_{0I} (Hz)	ω_{0O} (Hz)	ω_{0I}/ω_{0O}
0	0.103	−0.094	0.023	0.058	0.080	0.104	0.044	3987.0	3994.0	0.9983
	−0.394	−0.196	−1.610	0.184	0.167	−0.127	−0.241			
$2\pi/7$	−0.090	−0.187	−0.114	−0.084	−0.100	−0.151	−0.056	4012.7	4013.8	0.9997
	0.172	0.119	−0.253	−0.153	−0.160	0.106	0.231			
$4\pi/7$	−0.695	−0.957	−0.664	−0.463	−0.873	−0.835	−0.485	4099.9	4081.4	1.0045
	0.001	−0.023	−0.065	−0.015	−0.010	0.011	0.015			
$6\pi/7$	0.162	0.233	0.238	0.138	0.233	0.249	0.130	3969.7	3980.6	0.9973
	0.239	0.148	0.113	0.015	0.011	−0.011	−0.016			
$8\pi/7$	0.766	1.237	0.826	0.594	1.066	1.071	0.591	3879.8	3911.5	0.9919
	0.079	−0.003	0.022	−0.016	−0.011	0.011	0.016			
$10\pi/7$	−0.198	−0.337	−0.205	−0.168	−0.333	−0.302	−0.185	4031.9	4028.6	1.0008
	−0.036	0.037	0.088	0.103	0.065	−0.072	−0.094			
$12\pi/7$	−0.173	−0.268	−0.228	−0.168	−0.240	−0.302	−0.133	4027.5	4025.3	1.0006
	0.283	−0.004	0.275	0.038	0.033	−0.026	−0.048			
0	0.100	0.221	0.051	0	0.159	0.209	0	3928.3	3990.4	0.9980
	−0.465	−0.084	−0.605		0.167	−0.127				
0	0.116	0.267	0.067	0	0.196	0.245	0	3979.4	3988.1	0.9978
	−0.400	−0.069	−0.458		0.136	−0.108				
0	0.132	0.313	0.084	0	0.233	0.282	0	3976.4	3985.8	0.9976
	−0.350	−0.059	−0.368		0.114	−0.094				

Secondly, by not distributing the trimming masses evenly around the circumference of the ring, the total size of the trimming mass applied to the ring can be reduced. Compare the set of trimming masses applied at $\phi_1 = 6\pi/7$ and $8\pi/7$ with the last three sets of trimming masses. The reason that larger masses are required when the trimming masses are evenly distributed around the circumference of the ring is that the coupling introduced by individual trimming masses is largely negated by the other trimming masses. This is the principle that can be used to eliminate the frequency split between the in-plane and out-of-plane modes without introducing coupling. Therefore, only a small proportion of the coupling introduced by the trimming masses will remain unbalanced and it is this small proportion that negates the coupling introduced by the imperfection masses.

Fig. 9 shows the solutions to an incremental application of the second set of trimming masses in Table 4 (the set with the −0.090% mass at $2\pi/7$ radians). Considering only the first two sections of Fig. 9, it can be seen that the in-plane and out-of-plane frequency splits and the in-plane/out-of-plane coupling have again been successfully eliminated. Thus, Eqs. (86) and (87) can be used to produce larger trimming masses, applied within the cross-section of the ring, that will successfully trim the ring.

(iii) *Modification of the axial positions* (*Eqs.* (69)–(73)): This method for modifying the axial positions of the trimming masses involves making a modification to Eq. (73) similar to that made

to Eq. (64) by Eqs. (86) and (87). Specifically, for $i \neq j$ and $4 \leqslant i, j \leqslant N$, axial positions L_i and L_j can be modified to

$$L_i = \frac{\vartheta_2 G_1(m_3) - \vartheta_1 G_2(m_3) - b}{(N-3)(G_1(m_3)G_2(m_i) - G_2(m_3)G_1(m_i))},$$
$$L_i = \frac{\vartheta_2 G_1(m_3) - \vartheta_1 G_2(m_3) + b}{(N-3)(G_1(m_3)G_2(m_i) - G_2(m_3)G_1(m_i))}, \quad (88, 89)$$

where b is a constant value that is independent of the properties of the ring and the trimming masses. It is unlikely that it will be possible to reduce the axial positions of all of the trimming masses using this method alone. Instead, it could be used in conjunction with the other methods.

For example, the first of the five mass solutions in Table 4 (the set with the 0.100% mass at position 1) has a single trimming mass outside of the cross-section of the ring, specifically at an axial position of −6.05 mm. Using Eqs. (88) and (89), the axial positions of the five masses, reading from left to right, can be modified to −0.146, −0.119, 0.021, 0.278 and −0.043 mm without changing the size of any of the masses.

(iv) *General solution*: Consider Figs. 10(a) and (b). These have been generated from Eq. (67) using the same data that generated Fig. 9 with the exception that the out-of-plane angular positions, ϕ_{po}, were taken to be 15° and 45°, i.e., the out-of-plane sensors are no longer aligned with the out-of-plane generalized co-ordinates. With this alignment of the sensors and generalized co-ordinates, the analytical method previously used to determine the axial positions cannot be used. Instead, a graphical solution to Eq. (67) is required. Fig. 10(a) shows the initial curves that can be formed by varying the axial position of each of the trimming masses between $\pm L/2$ (i.e., ± 0.525 mm), whilst maintaining the axial position of the other trimming masses at $L/2$. It can be seen that some of the curves have a minimum value at $L/2$ whilst other curves have a minimum within the range considered. By determining the axial position of the trimming mass at which the minimum of Fig. 10(a) occurs and fixing the axial position of the relevant trimming mass, a further set of curves can be generated with a new set of minima. This process would continue until a minimum is found with respect to all trimming masses such as the situation shown in Fig. 10(b), which has been generated using the axial positions calculated by the previous method to fix the positions of the trimming masses that are not being varied in each curve.

Thus, it has been shown that the methods derived in Section 3.2 to eliminate the in-plane/out-of-plane coupling can be applied successfully.

4.3. Matching the in-plane and out-of-plane natural frequencies

Consider the problem of matching the in-plane and out-of-plane natural frequencies without introducing coupling into the ring. This can be observed from the final third of Fig. 9. After the first set of trimming masses were applied to the ring, the in-plane modes had a natural frequency of 4012.7 Hz whilst the out-of-plane modes had a natural frequency of 4013.8 Hz according to the approximate solutions. Including the effect of h_i^2 and L_i^2, it can be seen, from Fig. 9(e), that there is a small difference between the exact and approximate out-of-plane natural frequencies, of about 0.1 Hz. The size of the second set of trimming masses will be determined from the approximate solutions, which is the reason that it takes 100% of the second set of trimming masses to match the approximate in-plane and out-of-plane natural frequencies but 110% to match the exact

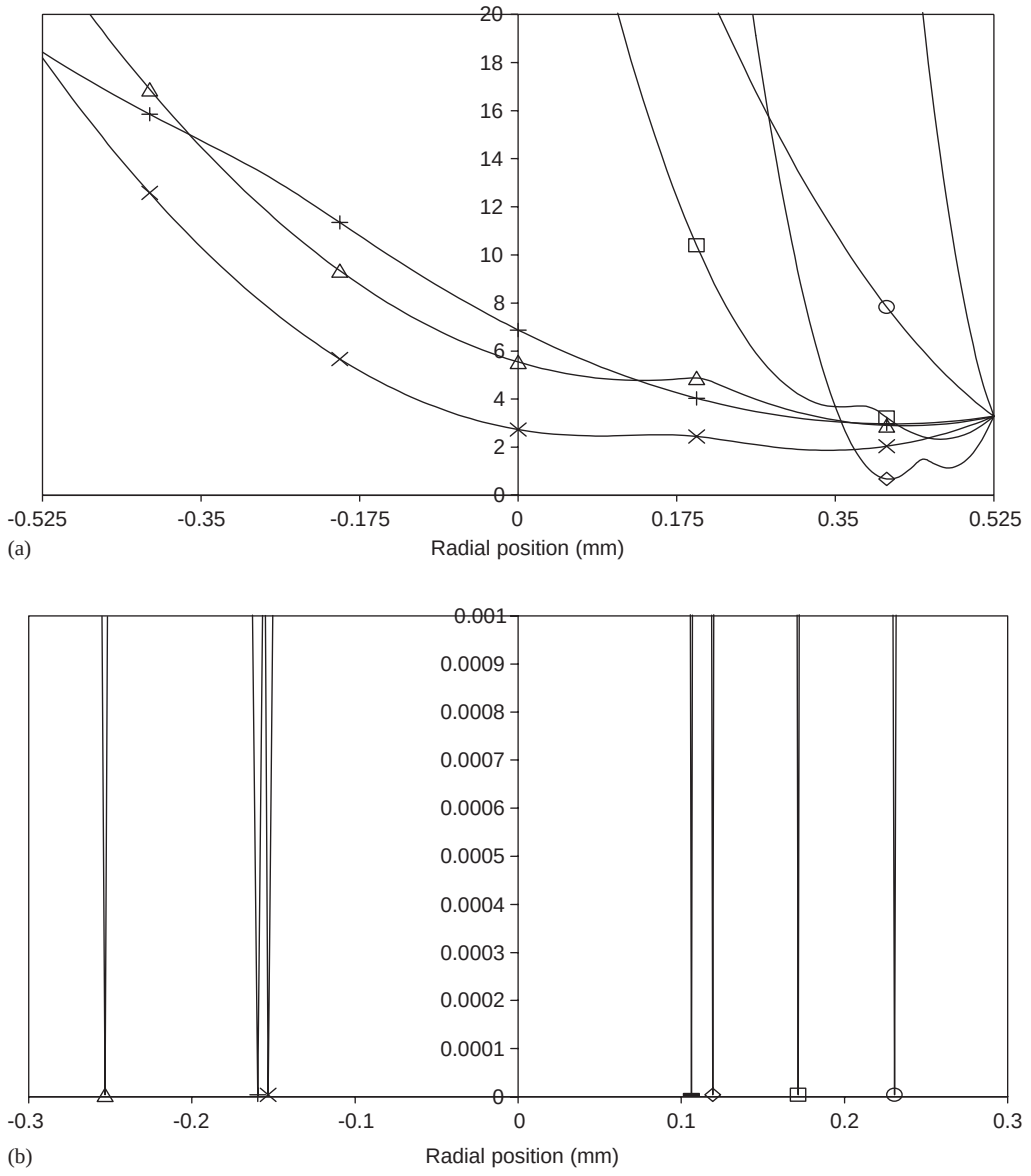

Fig. 10. (a) Initial set of solutions to Eq. (67) for the second set of trimming masses in Table 4 with variations in the axial positions L_i ($\square, L_1$; $\diamond, L_2$; $\triangle, L_3$; $\times, L_4$; $+, L_5$; $-, L_6$; $\bigcirc, L_7$). $L_j = L/2$ if $j \neq i$. (b) Final set of solutions to Eq. (67) for the second set of trimming masses in Table 4 with variations in the axial positions L_i ($\square, L_1$; $\diamond, L_2$; $\triangle, L_3$; $\times, L_4$; $+, L_5$; $-, L_6$; $\bigcirc, L_7$). The value of L_j is given in Table 4 if $j \neq i$.

in-plane and out-of-plane natural frequency. However, even at 100% of the trimming masses the difference between the exact in-plane and out-of-plane natural frequencies is 0.1 Hz, which is a difference of less than 0.01%.

To produce the final third of Fig. 9, seven regularly spaced trimming masses were removed from the ring. The magnitude of these seven masses were calculated using Eq. (83) with the radial

position of the masses being $-h/2$ and so the second set of trimming masses each need to be 0.0351% of the mass of the trimmed ring, or 0.0349% of the mass of the perfect ring. The masses were all attached to the ring at an axial position of 0 so as to introduce no additional coupling between the in-plane and out-of-plane generalized co-ordinates. In the final third of Fig. 9, the proportion of the trimming masses applied to the ring is increased from 0% to 100% with 100% of the imperfection masses applied at every point and the trimming masses from Stage 1 also applied at every point.

It can be seen from Figs. 9(a)–(d) that some coupling between the in-plane and out-of-plane generalized co-ordinates will reappear as the difference between the in-plane and out-of-plane natural frequency decreases. This is because the curves have been generated using approximate solutions, not exact solutions. However, as has already been noted, the difference between the in-plane and out-of-plane natural frequencies is small, i.e., less than 0.01%, by the point that the coupling becomes significant, as can be seen from Fig. 9(e).

Hence, it has been shown that it is possible to eliminate the frequency splits between the in-plane and out-of-plane modes of vibration whilst maintaining the predominantly in-plane and out-of-plane nature of the two pairs of modes.

5. Conclusions

A method for eliminating natural frequency splits between a pair of in-plane modes and a pair of out-of-plane modes of an imperfect ring has been proposed. In contrast to previous work, account has been taken of any coupling between the in-plane and out-of-plane modes, ensuring that the trimmed modes are pure in-plane and pure out-of-plane modes. The proposed mass trimming method is performed in 3 stages. Stage 1 eliminates the frequency split between a pair of predominantly in-plane modes and a pair of predominantly out-of-plane modes. Stage 2 eliminates any cross-coupling between the in-plane and out-of-plane modes. Stage 3 matches all four of the in-plane and out-of-plane natural frequencies together. Numerical results indicate that it is theoretically possible to trim the natural frequencies using the proposed method. Further work is needed to experimentally validate the proposed method.

Acknowledgements

The authors gratefully acknowledge the support for this work provided by BAE SYSTEMS and EPSRC under the Industrial CASE scheme.

Appendix A

$$\zeta_{ij} = (1 + 2h_i n_O^2 \xi) \sin 2n_I(\phi_j - \varphi_{n_I}) \sin 2n_O(\phi_i - \varphi_{n_O}) - (1 + 2h_j n_O^2 \xi) \sin 2n_I(\phi_i - \varphi_{n_I}) \sin 2n_O(\phi_j - \varphi_{n_O}), \quad \text{(A.1)}$$

$$\begin{aligned}\chi_i = &(1+2h_1 n_O^2\xi)\sin 2n_I(\phi_2-\phi_i)\sin 2n_O(\phi_1-\varphi_{n_o})\\ &+ (1+2h_2 n_O^2\xi)\sin 2n_I(\phi_i-\phi_1)\sin 2n_O(\phi_2-\varphi_{n_o})\\ &+ (1+2h_i n_O^2\xi)\sin 2n_I(\phi_1-\phi_2)\sin 2n_O(\phi_i-\varphi_{n_o}),\end{aligned} \tag{A.2}$$

$$\kappa_i = \Xi_1(\zeta_{2i}\chi_3-\zeta_{23}\chi_i),\quad +\Xi_2(\zeta_{i1}\chi_3-\zeta_{31}\chi_i),\quad -\Xi_3\zeta_{12}\chi_i + x_i\zeta_{12}\chi_3, \tag{A.3}$$

$$\tau_\Xi = \zeta_{12}\begin{pmatrix} \Lambda_{n_O}\chi_3 \\ -\lambda_{n_I}(\Xi_1\zeta_{23}+\Xi_2\zeta_{31}+\Xi_3\zeta_{12})\end{pmatrix}, \tag{A.4}$$

$$G_{I1O1} = -m_i\cos n_I(\phi_i-\varphi_{n_I})\cos n_O(\phi_i-\varphi_{n_o}), \tag{A.5}$$

$$G_{I1O2} = -m_i\cos n_I(\phi_i-\varphi_{n_I})\sin n_O(\phi_i-\varphi_{n_o}), \tag{A.6}$$

$$G_{I2O1} = m_i\sin n_I(\phi_i-\varphi_{n_I})\cos n_O(\phi_i-\varphi_{n_o}), \tag{A.7}$$

$$G_{I2O2} = m_i\sin n_I(\phi_i-\varphi_{n_I})\sin n_O(\phi_i-\varphi_{n_o}), \tag{A.8}$$

$$\vartheta_{I1O1} = \frac{V(F_{I1},\varphi_{n_o})}{W(F_{I1},\phi_{pi})}\frac{(M_{O1}+m_{O1})}{n_O^2\xi}\frac{((\omega_{O1}^2-\omega^2)^2+4\omega^2\omega_{O1}^2\gamma_{O1}^2)^{1/2}}{\omega^2}\cos n_I(\phi_{pi}-\varphi_{n_I}), \tag{A.9}$$

$$\vartheta_{I1O2} = \frac{V(F_{I1},\varphi_{n_o}+\pi/2n_O)}{W(F_{I1},\phi_{pi})}\frac{(M_{O2}+m_{O2})}{n_O^2\xi}\frac{((\omega_{O2}^2-\omega^2)^2+4\omega^2\omega_{O2}^2\gamma_{O2}^2)^{1/2}}{\omega^2}\cos n_I(\phi_{pi}-\varphi_{n_I}), \tag{A.10}$$

$$\vartheta_{I2O1} = \frac{V(F_{I2},\varphi_{n_o})}{W(F_{I2},\phi_{pi})}\frac{(M_{O1}+m_{O1})}{n_O^2\xi}\frac{((\omega_{O1}^2-\omega^2)^2+4\omega^2\omega_{O1}^2\gamma_{O1}^2)^{1/2}}{\omega^2}\sin n_I(\phi_{pi}-\varphi_{n_I}), \tag{A.11}$$

$$\vartheta_{I2O2} = \frac{V(F_{I2},\varphi_{n_o}+\pi/2n_O)}{W(F_{I2},\phi_{pi})}\frac{(M_{O2}+m_{O2})}{n_O^2\xi}\frac{((\omega_{O2}^2-\omega^2)^2+4\omega^2\omega_{O2}^2\gamma_{O2}^2)^{1/2}}{\omega^2}\sin n_I(\phi_{pi}-\varphi_{n_I}), \tag{A.12}$$

$$\begin{aligned}G_k(m_i) = &G_{I1O1}(m_i)(G_{I1O2}(m_1)G_{I2Ok}(m_2)-G_{I2Ok}(m_1)G_{I1O2}(m_2))\\ &+ G_{I1O2}(m_i)(G_{I2Ok}(m_1)G_{I1O1}(m_2)-G_{I1O1}(m_1)G_{I2Ok}(m_2))\\ &+ G_{I2Ok}(m_i)(G_{I1O1}(m_1)G_{I1O2}(m_2)-G_{I1O2}(m_1)G_{I1O1}(m_2)),\end{aligned} \tag{A.13}$$

$$\begin{aligned}\vartheta_k = &\vartheta_{I1O1}(G_{I1O2}(m_1)G_{I2Ok}(m_2)-G_{I2Ok}(m_1)G_{I1O2}(m_2))\\ &+ \vartheta_{I1O2}(G_{I2Ok}(m_1)G_{I1O1}(m_2)-G_{I1O1}(m_1)G_{I2Ok}(m_2))\\ &+ \vartheta_{I2Ok}(G_{I1O1}(m_1)G_{I1O2}(m_2)-G_{I1O2}(m_1)G_{I1O1}(m_2)).\end{aligned} \tag{A.14}$$

References

[1] R. Eley, C.H.J. Fox, S. McWilliam, Coriolis coupling effects on the vibration of rotating rings, *Journal of Sound and Vibration* 238 (3) (2000) 459–480.

[2] R. Eley, Ph.D. Thesis, University of Nottingham, UK, 2000.

[3] T. Fujita, K. Maenaka, T. Mizuno, T. Matsuoka, T. Kojima, T. Oshima, M. Maeda, Disk-shaped bulk micromachined gyroscope with vacuum sealing, *Sensors and Actuators A* 82 (2000) 198–204.
[4] C.P. Fell, C.H.J. Fox, Vibratory structure gyroscope, UK Patent GB 2335273, 2002.
[5] C.P. Fell, C.H.J. Fox, Two axis gyroscope, UK Patent GB 2338781, 2002.
[6] R. Eley, C.H.J. Fox, C.P. Fell, S. McWilliam, A multi-axis rate sensor based on a vibrating ring structure, *Proceedings of DGON Symposium on Gyro Technology*, Stuttgart, 2001.
[7] B.J. Gallacher, J.S. Burdess, A.J. Harris, M.E. McNie, The design and fabrication of a multi axis vibrating ring gyroscope, *Proceedings of DGON Symposium on Gyro Technology*, Stuttgart, 2001.
[8] S.A. Tobias, A theory of imperfection for elastic bodies of revolution, *Engineering* 172 (1951) 409–410.
[9] R. Perrin, Selection rules for the splitting of the degenerate pairs of natural frequencies of thin circular rings, *Acustica* 25 (1971) 69–72.
[10] T. Charnley, R. Perrin, Perturbation studies with a thin circular ring, *Acustica* 28 (1973) 139–146.
[11] P.A.A. Laura, C.P. Filipich, R.E. Rossi, J.A. Reyes, Vibrations of rings of variable cross section, *Applied Acoustics* 25 (1988) 225–234.
[12] R.F. Tonin, D.A. Bies, Free vibration of a circular cylinder with variable thickness, *Journal of Sound and Vibration* 62 (1979) 165–180.
[13] C.H.J. Fox, A simple theory for the analysis and correction of frequency splitting in slightly imperfect rings, *Journal of Sound and Vibration* 142 (3) (1990) 227–243.
[14] C.H.J. Fox, Mode trimming in nominally axi-symmetric structures, *Proceedings of XV International Modal Analysis Conference*, Tokyo, 1997, pp. 566–572.
[15] R.S. Hwang, C.H.J. Fox, S. McWilliam, The in-plane vibration of thin rings with in-plane profile variations, Part I: general background and theoretical formulation, *Journal of Sound and Vibration* 220 (3) (1999) 497–516.
[16] C.H.J. Fox, R.S. Hwang, S. McWilliam, The in-plane vibration of thin rings with in-plane profile variations, Part II: application to nominally circular rings, *Journal of Sound and Vibration* 220 (3) (1999) 517–539.
[17] R.S. Hwang, C.H.J. Fox, S. McWilliam, Free vibrations of elliptical rings with circumferentially variable thickness, *Journal of Sound and Vibration* 228 (3) (1999) 683–699.
[18] R. Eley, C.H.J. Fox, S. McWilliam, Anisotropy effects on the vibration of circular rings made from crystalline silicon, *Journal of Sound and Vibration* 228 (1) (1999) 11–35.
[19] A.K. Rourke, S. McWilliam, C.H.J. Fox, Multi-mode trimming of imperfect rings, *Journal of Sound and Vibration* 248 (4) (2001) 695–724.
[20] A.K. Rourke, S. McWilliam, C.H.J. Fox, Multi-mode trimming of imperfect rings using masses at pre-selected locations, *Journal of Sound and Vibration* 256 (2) (2002) 319–345.
[21] J. Kirkhope, Out-of-plane vibration of thick circular ring, *Journal of the Engineering Mechanics Division* 102 (1976) 239–247.
[22] Blevins, *Formulas for Natural Frequencies and Mode Shapes*, Krieger, Malabar, FL, 1995.
[23] A.K. Rourke, Ph.D. Thesis, University of Nottingham, UK, 2002.